CHARACTERIZATION OF DIELECTRIC BARRIER DISCHARGE PLASMA ACTUATORS FOR FLOW SEPARATION CONTROL

A THESIS

Presented in Partial Fulfillment of the Requirements for

Graduation with Distinction in the

Department of Mechanical Engineering at

The Ohio State University

By

Timothy P. Munther

****

The Ohio State University

May 2007

Examination Committee:

Dr. Mo Samimy, Advisor

Dr. Igor Adamovich

Approved by

_____

Advisor

Department of Mechanical Engineering

ABSTRACT

The application of dielectric barrier discharge (DBD) plasma actuators for separation control is an innovative technology which can significantly enhance aircraft performance by eliminating excess weight and reducing the mechanical complexity of current flow control systems. This research presents a study on the development and characterization of (DBD) plasma actuators that will be later implemented to actively control flow separation over a high-lift airfoil. The frequency, applied voltage, dielectric material, and ballast resistance were varied in order to identify their effects on plasma formation, electrical power, and induced flow. The most notable trends observed were at higher frequencies and voltages stronger plasma was formed and a higher velocity was induced.

ACKNOWLEDGEMENTS

I would like to thank Professor M. Samimy for this research opportunity and his academic guidance during this project. I would like to thank Professor Adamovich for his assistance. I would also like thank Jesse Little for his tremendous help with the data analysis as well as the PIV measurements and Munetake Nishihara for his work with the electrical measurements. Additionally, I would like to extend thanks to Edgar Caraballo, Jeff Kastner, and Doug Mitchell for their helpful discussions.

TABLE OF CONTENTS

LIST OF FIGURES

LIST OF TABLES

1 INTRODUCTION

There are critical times during flight when the control of flow separation over aircraft wings is of highest concern. This most commonly occurs during takeoff, landing, or, with agile aircraft, while performing difficult maneuvers. Such instances generally use large angles of attack and/or flap deflection to modify the aerodynamic forces on the vehicle. The modifications often come at the expense of flow separation over deflected surfaces. When this occurs, the accompanying drastic loss in lift and increase in pressure drag can negatively affect aircraft performance. Consequently, controlling or eliminating flow separation is a point of immense interest for enhancement of aircraft performance and efficiency.

A few control methods fall under the general category of active control and have extremely attractive prospects in comparison with the conventional passive control techniques. In particular, active control using DBD plasma actuators has tremendous potential for controlling flow separation. Recent research has shown that the flow inducing effects of these actuators can be used to introduce momentum into the boundary layer in order to delay separation and thus increase the maximum value of the coefficient of lift in some circumstances [1].

At The Ohio State University, the capabilities of DBD plasma actuation are being researched for separation control applications. The work presented in this thesis focuses on a characterization of DBD plasma actuators. Various parameters that affect plasma formation and the flow inducing characteristics of the actuators are analyzed. After a more thorough understanding of how plasma actuators function and under what

conditions they are most effective, the actuators will be applied to a high-lift airfoil that exhibits a single trailing edge flap.

2 BACKGROUND

2.1 Flow Separation

As air flows over an airfoil, a boundary layer forms near the surface of the airfoil. When the boundary layer remains attached to the surface, a low pressure region above the airfoil and high pressure region below the airfoil create lift. This comes at the expense of kinetic energy losses in the boundary layer on top of the airfoil caused by viscous effects near the airfoil's surface and an adverse pressure gradient that develops as the flow follows the airfoil surface curvature. These effects slow the fluid in the boundary layer until it reaches a critical value at which separation occurs. When the flow separates, the low pressure region above the airfoil becomes near atmospheric. The outcome is a severe loss in lift known as stall that is also accompanied by an increase in the pressure drag on the airfoil. This undesirable behavior considerably decreases efficiency and in some instances prevents the possibility of flight. Hence, controlling when and where flow separation occurs along an airfoil (or virtually any other aerodynamic structure) is of high interest.

2.2 Passive Control Techniques

Control methods that utilize geometric modifications are called passive control techniques. Passive flow control for aircraft wings include leading edge slats, trailing edge slotted flaps, or a combination of the two. These geometric modifications allow for some mixing to take place between flow from the high pressure region and flow from the low pressure region. This mixes the high and low momentum fluid and prevents flow

separation by reenergizing the boundary layer. The disadvantages of current designs are that they add mechanical complexity to the wing design, take up volume when not in use, add weight, and generate vibration and noise.

Another passive flow control device is the vortex generator. These are relatively small rigid fixtures that are placed on the top surface of an airfoil. When flow passes over them, they generate vortices. These vortices help mix free stream momentum into the boundary and thus delay flow separation along the airfoil. However, vortex generators increase drag, and due to their nature of being fixed on the surface of the airfoil, they decrease the efficiency of the flight when they are not needed.

2.3 Active Control Techniques

Active control methods involve adding mass or energy to the system. Compared to passive control, active control provides the potential for much more efficient means of controlling separation because they can be turned off by command. A variety of active control methods are undergoing research. One example is synthetic jets which utilize piezoelectric devices. This type of actuator uses acoustic excitation to introduce momentum to the near wall region of the flow using a diaphragm that vibrates over a chamber. These actuators still need to be advanced significantly for real flight applications. In comparison to plasma actuators, synthetic jets are much more complex and are cumbersome to integrate within the body of the airfoil. This makes plasma actuators an attractive alternative for active flow control.

2.4 Plasma Actuators

Plasma actuation is a potentially advantageous technology for flow control

leading to eventually flight control and as a result, much research has been devoted to this subject. Forte et al. have conducted research analyzing the effects of actuator geometry, material, input voltage, frequency, and other parameters [2]. Additionally, Corke and Post have applied DBD plasma actuators to multi-element wings and wings with movable control surfaces [1]. Santhanakrishnan et al. have compared and contrasted other forms of active flow control to plasma actuators [3].

The DBD plasma actuators that this research focused on are comprised of two rectangular electrodes asymmetrically aligned that sandwich a dielectric material (Figure 2.1). When a high AC voltage is applied to the electrodes, a weakly ionized region air, or plasma, forms over the insulated electrode. Also, due to the applied voltage an electric field exists between the two electrodes. When the plasma is in the presence of this electric field a body force is induced on the nearby air [1].

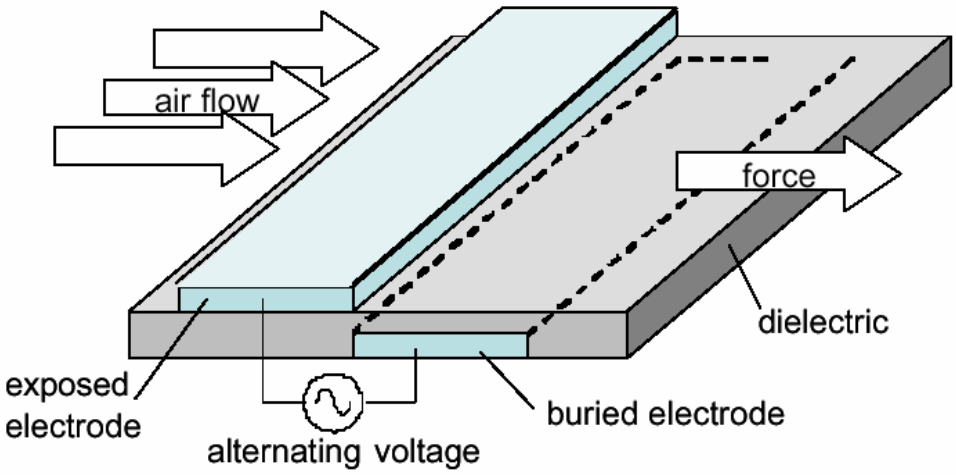

Figure 2.1 Schematic of a DBD Plasma Actuator [4]

Enloe et al. have performed many experiments to characterize the temporal and spatial features of single-dielectric-barrier-discharge plasma actuators [5-6]. A series of

microdischarges on the order of tens of nanoseconds comprise the plasma as charge is transferred back and forth between the dielectric and the exposed electrode [6]. An important feature of DBD plasma is that it can "sustain a large-volume discharge at atmospheric pressure without the discharge's collapsing into a constricted arc" [5]. The plasma maintains a bluish glow rather than a collapsed arc because of the self-limiting nature of the device caused by the dielectric material between the electrodes [5]. As a result, the microdischarges spread relatively uniformly along the electrodes rather than arc at an isolated location [6]. Furthermore, the charge that is deposited onto the dielectric reduces the local electric field and thereby tends to stop discharges from occurring [6]. The voltage signal applied to the electrodes must continually change for the discharges to continue and therefore has to be an AC or pulsed DC signal [6].

The plasma has been shown to form in six well-defined steps for every cycle of the AC voltage that is applied [5]. The first three steps are the ignition, expansion, and quenching of the "forward stroke" (Figure 2.2). During this stage, the voltage signal is decreasing and electrons are being deposited onto the dielectric material from the exposed electrode. The next three steps are the ignition, expansion, and quenching of the "backward stroke," when electrons are flowing from the dielectric surface to the exposed electrode (Figure 2.2). In this stage, the voltage signal is increasing. The plasma is formed as the result of a series of these microdischarges as electrons transfer onto and off of the dielectric surface [5].

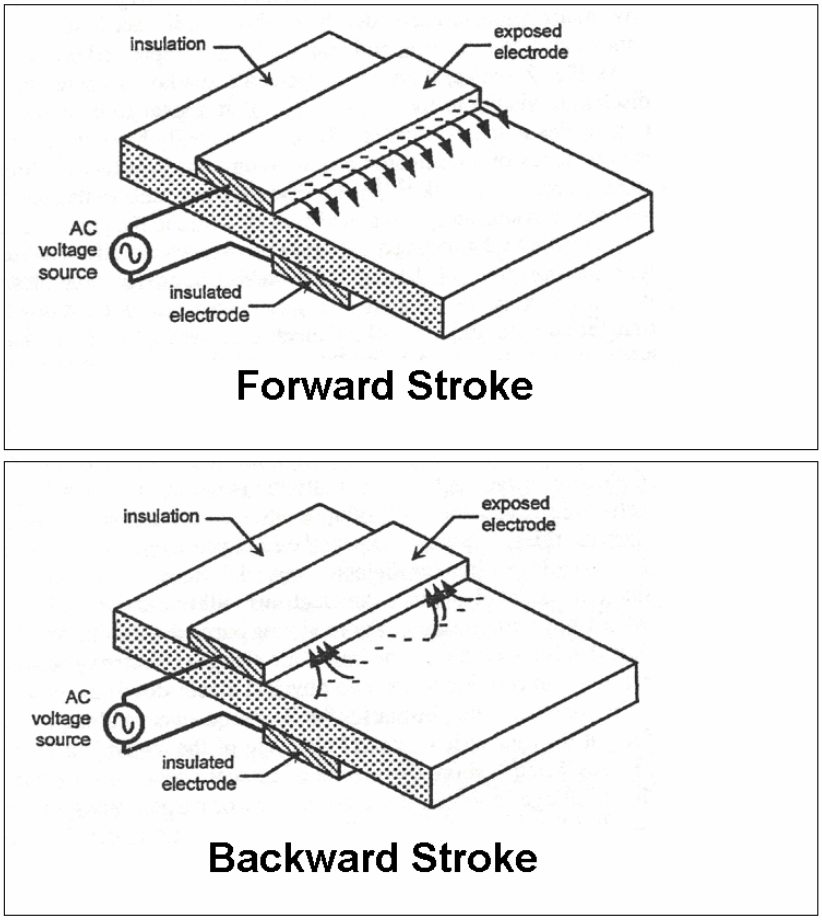

Figure 2.2: Forward and Backward Strokes of DBD Plasma Formation [5]

An electric field is created due to the high voltage applied to the electrodes, and the plasma in the presence of this field imposes a body force on the ambient air. Momentum is transferred to the flow at the near wall region by these ions interacting with the surrounding neutral air particles [6]. During the "forward stroke," the force opposes the flow, but during the "backward stroke," the force is in the flow direction. The force from the backward stroke is about five to twenty times stronger than the forward stroke [4]. Therefore, the net force is in the direction of from the exposed electrode toward the insulated electrode. This can be seen in Figure 2.3.

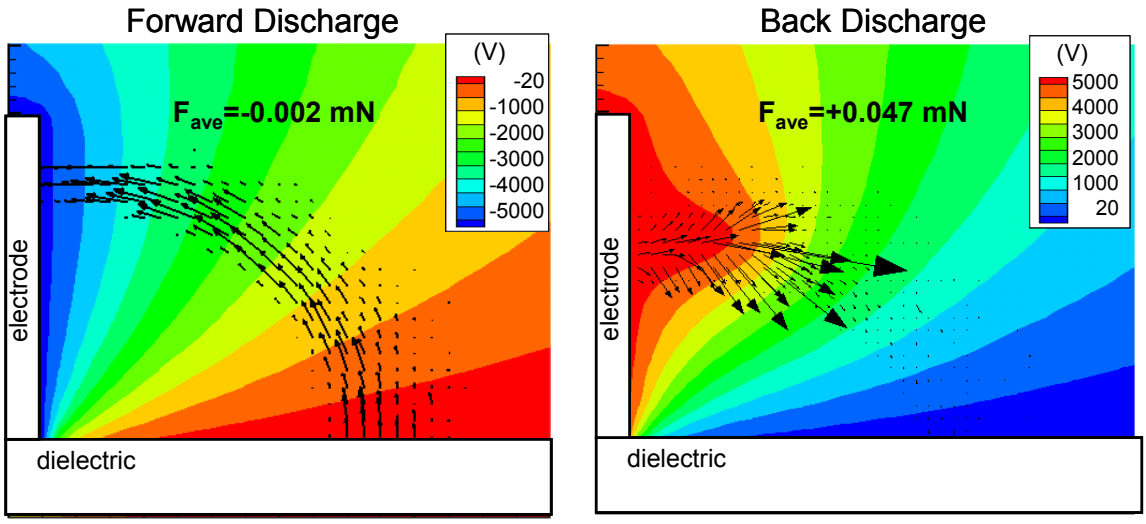

Figure 2.3: Voltage Profile and Average Force Values for Forward and Backward Strokes [4]

Applying DBD plasma actuators on airfoils is a relatively new method of controlling flow separation; nevertheless, recent experiments have shown positive results [1-6]. For leading edge separation control, Corke and Post have shown an almost a 15% increase in the maximum coefficient of lift by maintaining attached flow at higher angles of attack [1].

In aircraft applications, this technology could result in shorter takeoff and landing distances as well as increased flight efficiency. DBD plasma actuators are a low power device, and their design is extremely simplistic in comparison to other active control devices. Actuators can be flush mounted on the top surface of the airfoil and therefore do not contribute to unnecessary drag effects. The absence of moving parts is a valuable feature since the mechanical complexity of the airfoil's interior will be significantly reduced, eliminating excess weight.

3 EXPERIMENTAL METHODOLOGY

3.1 Experimental Facility

Experiments are performed at the Gas Dynamics and Turbulence Laboratory (GDTL) stationed at The Ohio State University's Don Scott Airport. A newly purchase recirculating wind tunnel is used to measure the flow inducing effect of the actuators (Figures 3.1 and 3.2). A Newport laser table close to the wind tunnel is used for the preliminary bench top experiments (Figure 3.3).

Figure 3.1: Recirculating Wind Tunnel

Figure 3.2: Test Section of Wind Tunnel

Figure 3.3: Newport Laser Table

3.2 Test Block

The plasma actuators were first implemented on a test block, which has the same finish and is constructed from the same material as the high-lift airfoil that will be used in the near future. The material is machineable and is called DuraForm®. This test block was purchased from General Pattern Co., Inc. and was manufactured by the rapid prototyping process referred to as selective laser sintering. The actuators were first characterized on the test block due to the fact that the airfoil is expensive and the effects of the plasma on the material were initially unknown. Therefore, if anything destructive occurred on the test block such as melting, burning, or degrading in some way, the proper precautions could be observed so as not to damage the airfoil.

A variety of views of the test block along with its dimensions can be seen in Figure 3.4. Figure 3.5 is a schematic of the plasma actuators on the block. In order to characterize the plasma actuators with flow, the actuators needed to be tested in the wind tunnel. Therefore, to facilitate smooth flow over the test block, an angle was machined into the leading edge (Figure 3.4).

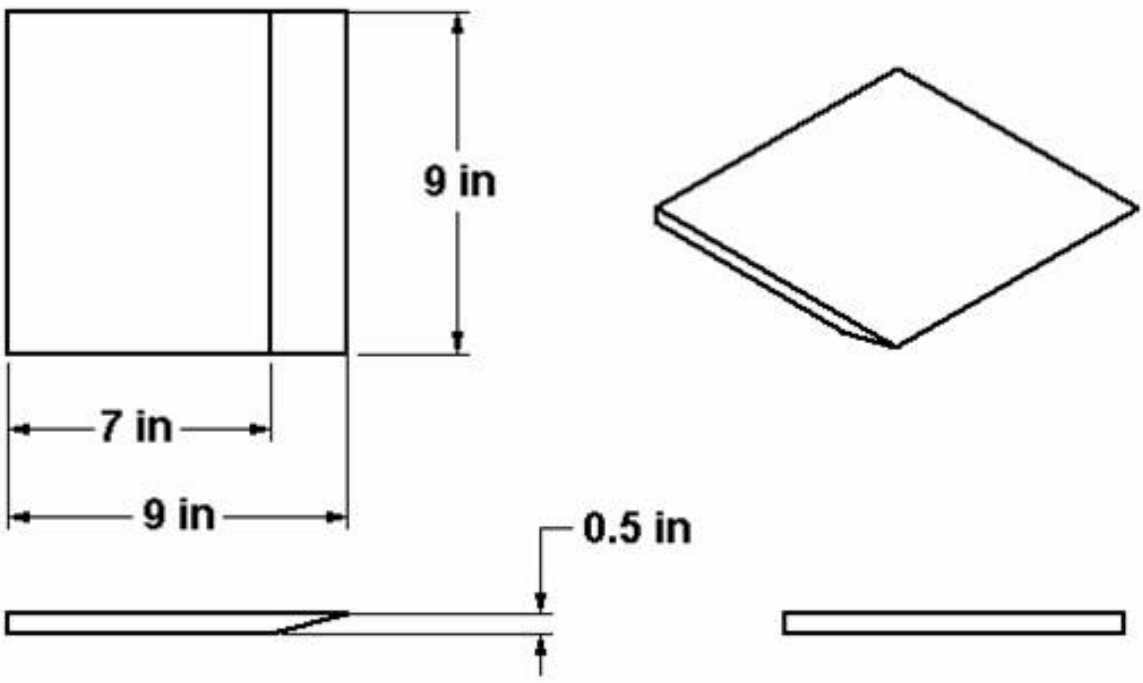

Figure 3.4: Technical Drawing of Test Block

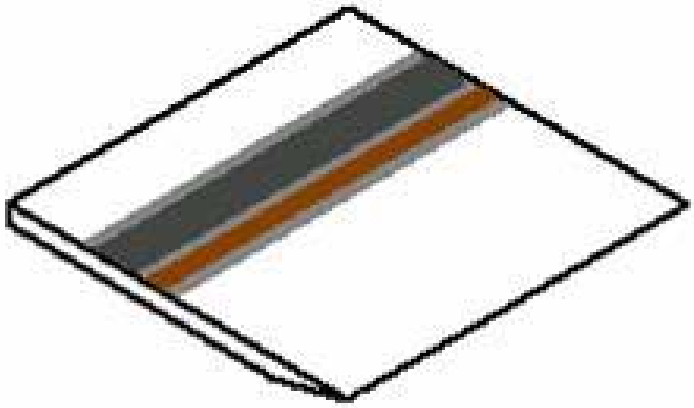

Figure 3.5: Schematic of Test Block with Plasma Actuator

3.3 Plasma Actuator Design

The plasma actuators are composed of two rectangular electrodes that sandwich a dielectric material. The electrodes are copper foil tape purchased from McMaster-Carr. The thickness of the copper foil is 0.0014 in., and the conductive adhesive of the tape has a thickness of 0.0021 in. Therefore, the total thickness of one electrode is 0.0035 in. The widths of the electrodes differ. The insulated, grounded electrode is 0.75 in wide where as the top, high voltage electrode is 0.25 in. The widths correspond to optimized conditions from the work of Forte et al. [2]. The electrodes span the substrate.

Two types of Teflon tape are used as a dielectric material. These were purchased from McMaster-Carr as well. The dielectric material is Teflon® Poly-Tetra-Fluoro-Ethylene (PTFE) and was recommended by Professor Jamey Jacob of Oklahoma State University. For the weaker dielectric which has a dielectric strength of 10 kV, the thickness of the Teflon® film is 0.003 in and the silicone adhesive is 0.0015 in, making a total thickness of 0.0045 in. For the stronger dielectric which has a dielectric strength of 21 kV, the thickness of the Teflon® film is 0.010 in and the silicone adhesive is 0.0015 in, making a total thickness of 0.0115 in. The width of both dielectric tapes is 2 inches, which is chosen to ensure that the copper electrodes are well within the edges of the dielectric.

The tapes are cut with scissors and are layered on top of each other in a parallel fashion with the 0.75 in wide electrode first, and then the dielectric, and finally the 0.25 in wide electrode (Figure 3.6). The gap between the electrodes was chosen to be 5 mm based upon the findings of Forte et al. Their research showed that the velocity attained a

maximum value given a gap width of about 5 mm [2]. The direction of the induced flow is from the high voltage electrode towards the grounded electrode.

In the initial design of the plasma actuators, the high voltage and ground leads were connected using alligator clips on the same side of the test block and the electrodes and dielectric were cut with square ends, as seen in Figures 3.6 and 3.7. The immediate problem encountered with this configuration was arcing at the corners of the electrodes, especially on the end where the leads were connected. This occurred since electrons tend to have a much higher concentration at sharp edges and corners. The adjustment for this problem led to a slightly altered design.

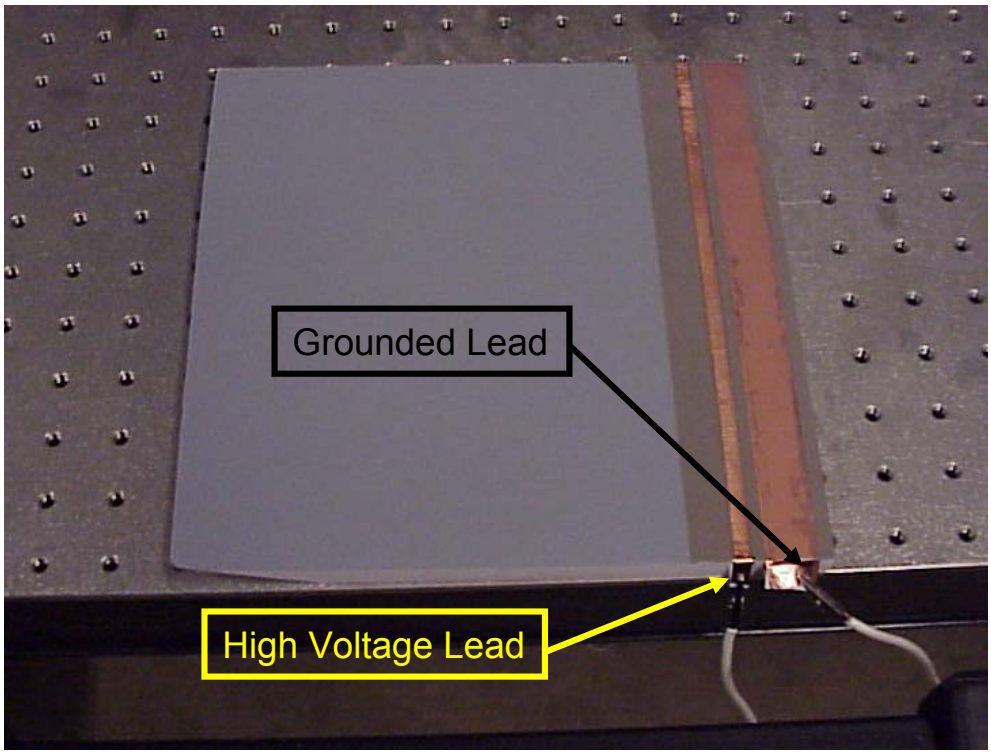

Figure 3.6: Initial Design of Plasma Actuator

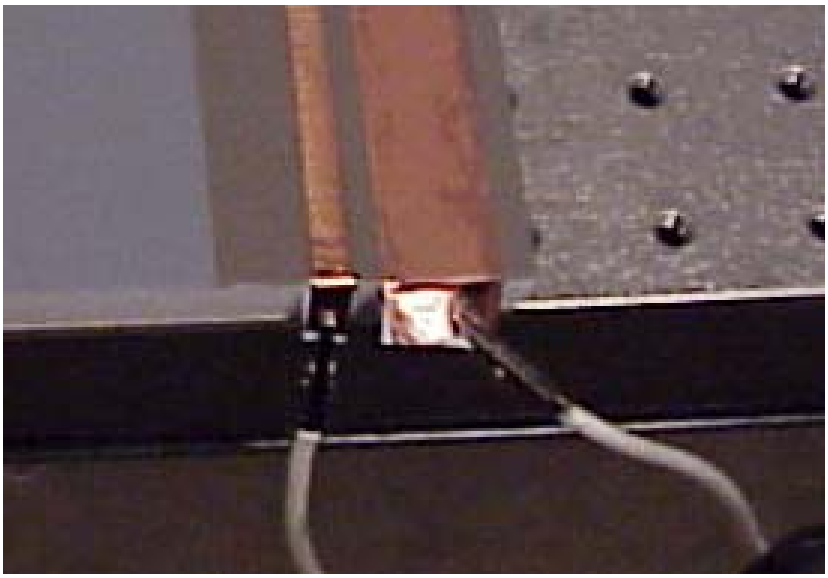

Figure 3.7: Leads Connected to Electrodes with Alligator Clips

The final design of the plasma actuators has rounded electrode ends to reduce the high concentration of electrons at potential sites of arcing. Moreover, since arcing tends to occur on the end where the leads are attached, the leads are connected to opposite sides. Figure 3.8 depicts the final design of the plasma actuators. The two plasma actuators only differ in regard to the dielectric used. One has a dielectric strength of 10 kV whereas the other has a dielectric strength of 21 kV. The two actuators are not operated simultaneously; they have been placed on the test block together to facilitate more efficient experimentation.

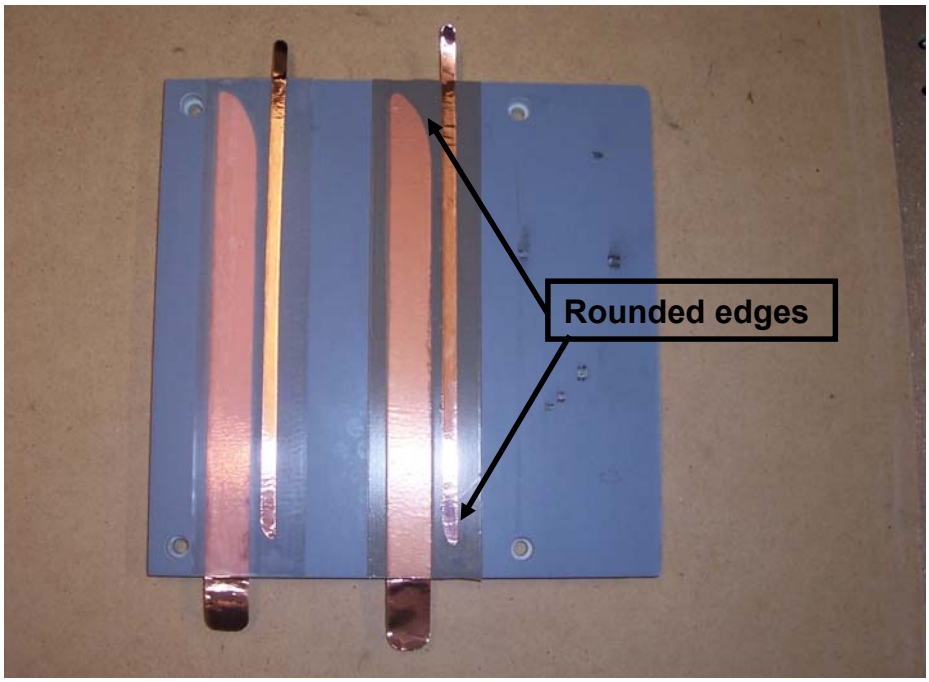

Figure 3.8: Final Design of Plasma Actuator

3.4 Experimental Setup

A BK Precision 3011A function generator (Figure 3.9) provides sinusoidal input signals to a Powertron 1500S AC power supply shown in Figure 3.10. Two of these power supplies are stored together, one on top of the other, in a metal shelf enclosure. The bottom power supply is used in this experimentation. The voltage signal from the power supply is stepped up to kilovolts scale by a transformer (Figure 3.11). The transformed is designed for frequencies in the range 1 to 10 kHz. This frequency range is similar to frequencies seen in the previous literature [1, 5-6]. The ballast resistors are of the high power ceramic type with resistance on the order of hundreds of kOhms (Figure 3.12). The high voltage signal was sent to the exposed electrode, and the insulated electrode was grounded.

Figure 3.9: BK Precision 3011A Function Generator

Figure 3.10: Powertron 1500S AC Power Supply

Figure 3.11: Transformer

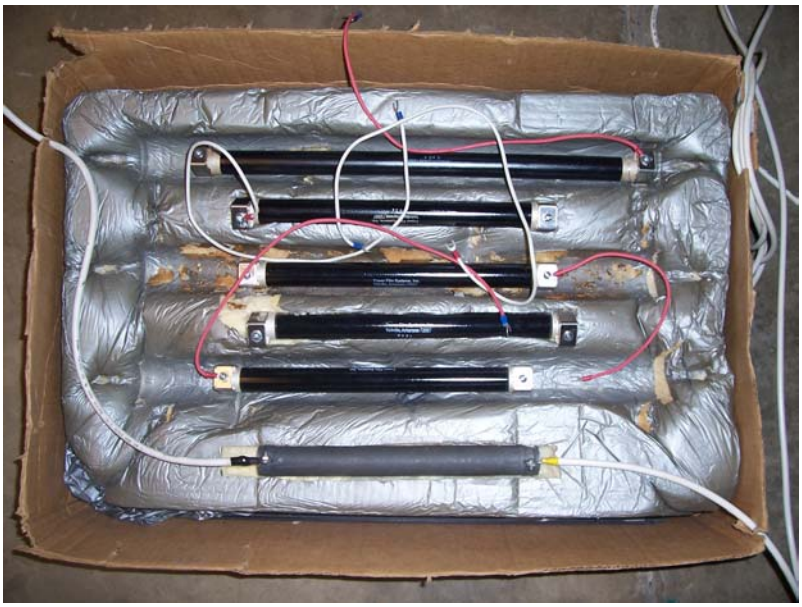

Figure 3.12: Ceramic Ballast Resistors

In order to measure the characteristics of the plasma, two slightly different circuits are used. One measures the current and high voltage traces, while the other measures charge and high voltage data. These two setups are discussed subsequently.

Initially, the IV measurements were obtained by the setup depicted in Figure 3.13. The schematic shows that the function generator sent an AC signal to the power supply.

The voltage of the signal was stepped up by the transformer to a voltage magnitude on the order of kilovolts. This voltage was applied the exposed electrode. The ballast resistors were connected in series with the insulated electrode, which was grounded.

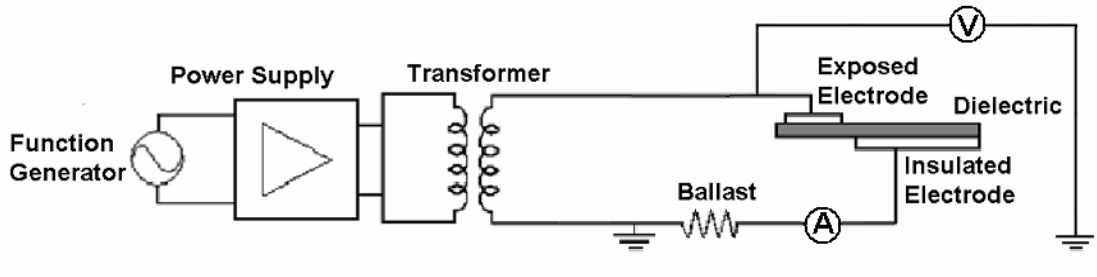

Figure 3.13: Initial Schematic for IV Measurements

The Agilent N2771A high voltage probe was set up to read the voltage across the uncovered electrode relative to ground. The LeCroy CP031 current probe was positioned to read the current in the lead coming from the insulated electrode. Data from the two probes are recorded on the LeCroy oscilloscope.

The main problem identified with the initial setup was that the current trace showed a significant capacitive current that caused problems with processing the data. This capacitive current was more noticeable as the frequency and voltage increased. By placing the ballast resistors in series with the high voltage electrode, the capacitive current effects were mitigated. With this new setup, which is shown in Figure 3.14, the capacitive current essentially vanished, and current traces more representative of those in the literature were obtained.

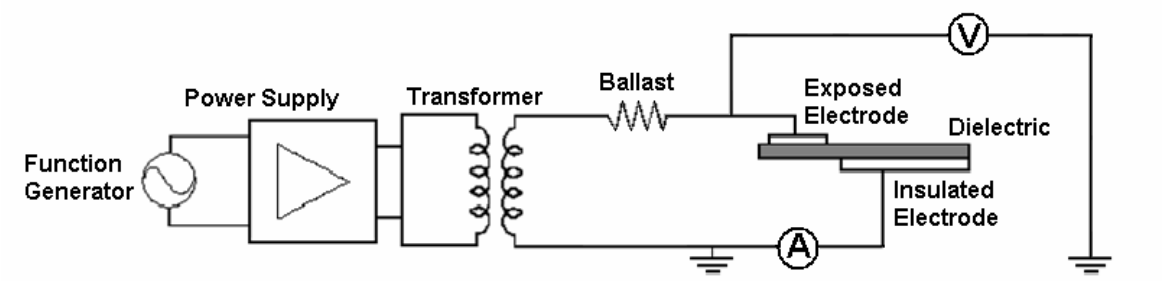

Figure 3.14: Final Schematic for IV Measurements

The QV measurements were obtained using the setup shown in Figure 3.15. Similar to the IV measurement setup, the function generator outputs an AC signal to the power supply. The voltage of the signal was then stepped up by the transformer and was applied the exposed electrode. The ballast resistors were connected in series with the exposed electrode. A 10 nF capacitor is placed between the insulated electrode and ground. The voltage reading across this capacitor was used to obtain the charge on the insulated electrode.

The voltage across the plasma actuator was read by the Tektronix P6015A voltage probe. The voltage across the capacitor was captured by Tektronix P6139A voltage probe. The data read by these two probes were recorded by the Tektronix oscilloscope. The Tektronix probes and oscilloscope were used since they showed less noise in the traces allowing for more accurate energy and power calculations.

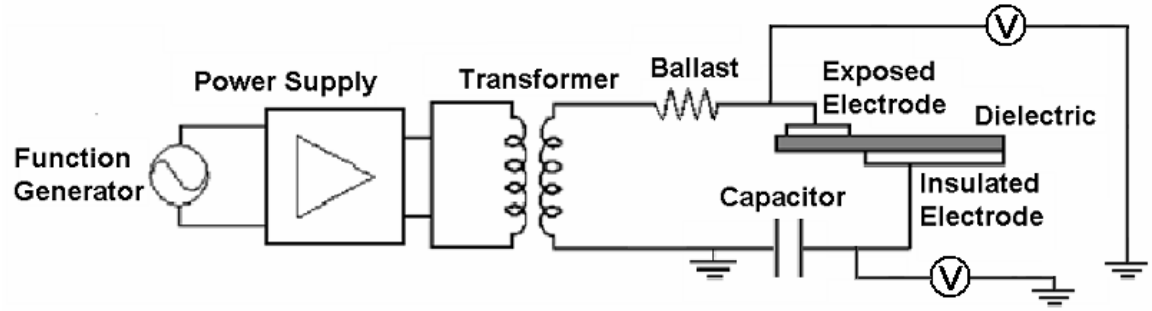

Figure 3.15: Schematic for QV Measurements

3.5 Data Acquisition

Two different data acquisition configurations are used to measure the current-voltage (IV) measurements and the charge-voltage (QV) measurements. Additional hardware is required for Particle Image Velocimetry (PIV) measurements. The following describes these setups.

The data acquired in the IV experiments are obtained with variety of instruments. Recordings of data for electrical property measurements are acquired simultaneously using a LeCroy Waverunner 6050A oscilloscope (Figure 3.16). The input voltage from the function generator is directly connected to the scope. In order to obtain the voltage applied to the electrodes, an Agilent N2771A high voltage probe that has an amplification factor of 1/1000 is used (Figure 3.17). This probe is connected to a ground on the laser table and positioned to read the voltage at the high voltage lead (Figure 3.18). In addition to measuring the voltage applied to the electrodes, the current is of specific interest since the spikes in the current signal are indicative of plasma formation. The current was obtained by a LeCroy CP031 current probe (Figure 3.19) that is attached between the encapsulated electrode and ground.

Figure 3.16: LeCroy Waverunner Oscilloscope

Figure 3.17: Agilent N2771A High Voltage Probe

Figure 3.18: LeCroy CP031 Current Probe

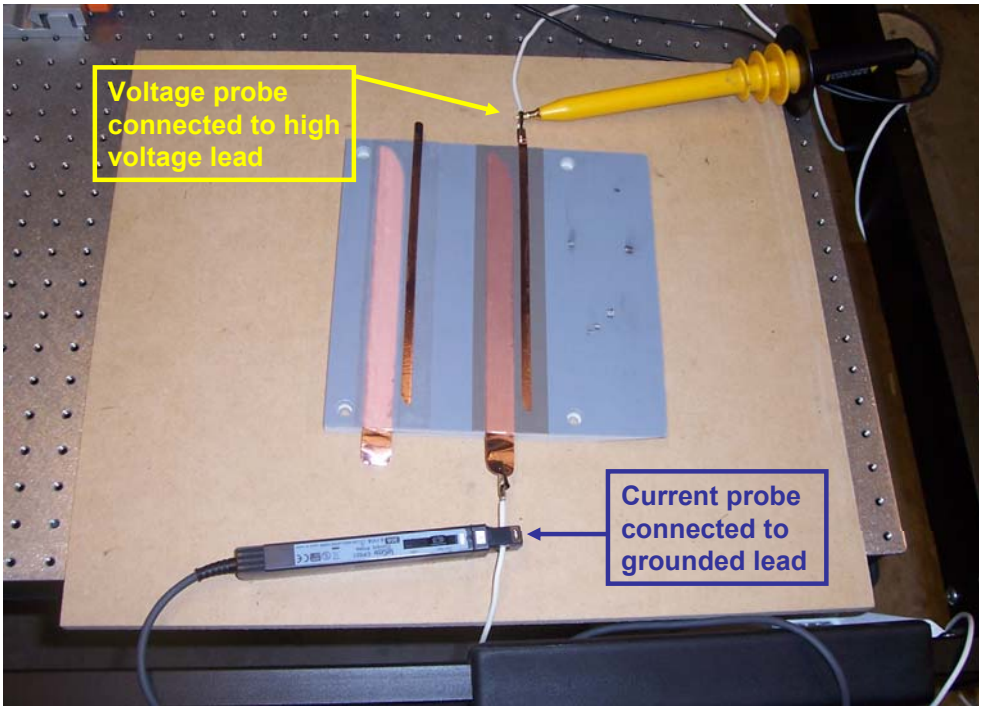

Figure 3.19: Setup with Voltage and Current Probes

The QV measurements used the following data acquisition tools. A Tektronix P6015A voltage probe with an amplification factor of 1/1000 is positioned to read the voltage at the high voltage lead (Figure 3.20). A Tektronix P6139A voltage probe is used

to measure the voltage across the capacitor (Figure 3.21). These two probes are connected to a Tektronix TDS 220 oscilloscope for simultaneous data acquisition (Figure 3.22).

Figure 3.20: Tektronix P6015A High Voltage Probe

Figure 3.21: Tektronix P6139A Voltage Probe

Figure 3.22: Tektronix TDS 220 Oscilloscope

The PIV data acquisition system utilized a LaVision Inc. PIV system with Imager Pro-X cameras and a dual-head Spectra Physics PIV-400 Nd:YAG laser. Figures 3.23 and 3.24 show the PIV setup and the test block in the wind tunnel. For a more thorough discussion regarding the details and calibration of the equipment see Little [7].

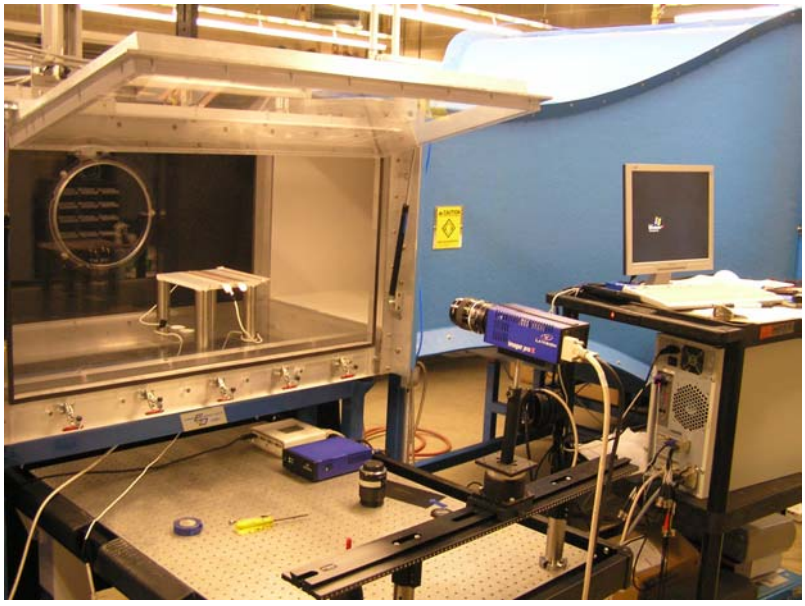

Figure 3.23: PIV Setup

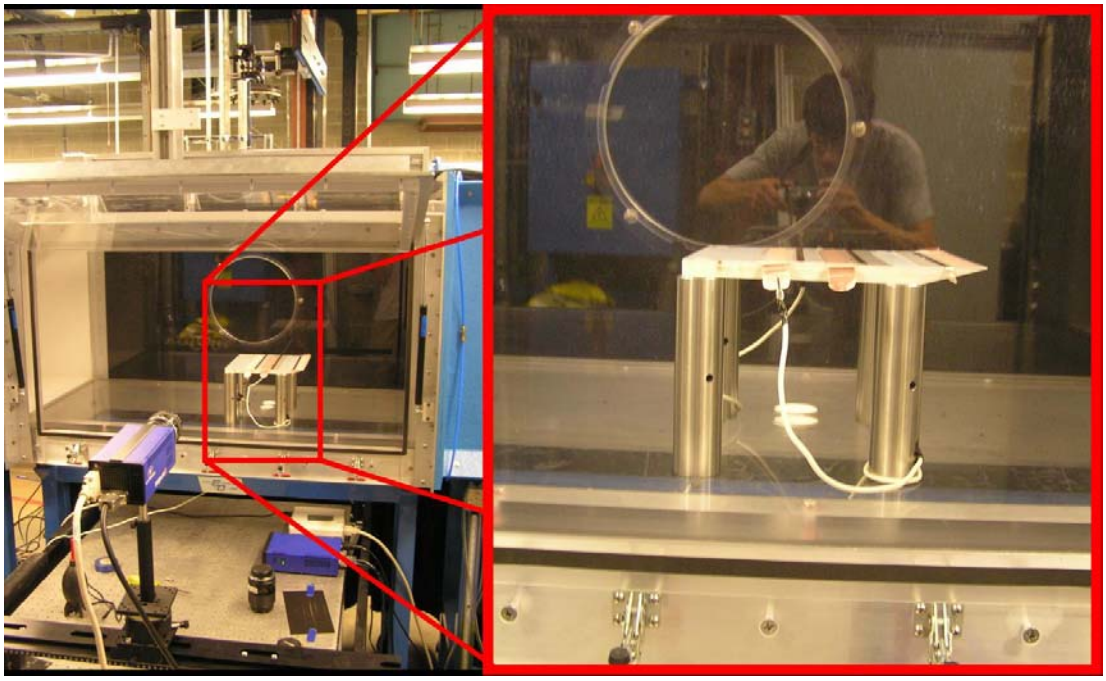

Figure 3.24: PIV Setup with Test Block

3.6 Test Matrix

Two different test matrices were developed for the characterization of the DBD plasma actuators. More runs were performed on the laser table than in the wind tunnel since the PIV experiments by nature are more complex and time consuming. The results from these bench top experiments are used to determine the interesting cases for PIV measurements.

Table 3.1 shows the parameters that were varied and held constant for the characterization of the plasma actuators. For the first ten runs, the effect of the frequency was studied on the two different dielectrics. The input voltage from the function generator was set to a nominal value of 1.36 V_{RMS}, and the ballast resistance was setup to be 100 kOhm, both of which were selected based upon preliminary results. The voltage that was applied to the exposed electrode can be seen in the far right column of Table 3.1.

The next ten runs analyzed the effect of changing the voltage on the two dielectrics, and the final four runs examined how the ballast resistance effects the plasma formation with only the dielectric with strength of 21 kV. For the IV measurements, no capacitor was used.

Given this test matrix, reasonable comparisons were drawn, both qualitatively and quantitatively, between voltage, frequency, dielectric, and ballast in regard to plasma formation and the electrical energy and power (see Results section).

Table 3.1: Test Matrix for IV and QV Measurements

Run	Frequency (kHz)	Dielectric Strength (kV)	Input Voltage from Function Generator (V_{RMS})	Ballast Resistance (kOhm)	High Voltage Applied to Exposed Electrode (kV_{RMS})	Capacitor (nF)
1	2	10	1.36	100	6.4	10
2	3	10	1.36	100	6.1	10
3	4	10	1.36	100	5.9	10
4	5	10	1.36	100	5.8	10
5	6	10	1.36	100	5.4	10
6	2	21	1.36	100	6.4	10
7	3	21	1.36	100	5.9	10
8	4	21	1.36	100	5.8	10
9	5	21	1.36	100	5.7	10
10	6	21	1.36	100	5.7	10
11	3	10	1.01	100	4.7	10
12	3	10	1.15	100	5.2	10
13	3	10	1.3	100	5.8	10
14	3	10	1.45	100	6	10
15	3	10	1.6	100	6.9	10
16	3	21	1.01	100	4.7	10
17	3	21	1.15	100	5.2	10
18	3	21	1.31	100	5.9	10
19	3	21	1.44	100	6.4	10
20	3	21	1.6	100	6.9	10
21	3	21	1.36	192	5.9	10
22	3	21	1.36	386	5.4	10
23	3	21	1.36	595	5	10
24	3	21	1.36	784	4.3	10

Due to time constraints, a more efficient test matrix was developed for the PIV measurements. Therefore, not all runs of the test matrix described in Table 3.1 were considered interesting in terms of PIV measurements due to negligible plasma formation. Specifically, input voltages less than 1.2 V_{RMS} (which corresponded to about 5.1 kV_{RMS} applied to the exposed electrode) as well as an increase in the ballast resistance above 100 kOhm were neglected. Table 3.2 shows the parameters that were tested when running the PIV setup.

Table 3.2: Test Matrix for PIV Measurements

Run	Frequency (kHz)	Dielectric Strength (kV)	Input Voltage from Function Generator (V_{RMS})	Ballast Resistance (kOhm)	High Voltage Applied to Exposed Electrode (kV_{RMS})	Capacitor (nF)
1	2	10	1.36	100	6.4	10
2	3	10	1.36	100	6.1	10
3	4	10	1.36	100	5.9	10
4	5	10	1.36	100	5.8	10
5	6	10	1.36	100	5.4	10
6	3	10	1.2	100	5.8	10
7	3	10	1.4	100	6.5	10
8	3	10	1.6	100	7	10
9	3	10	1.8	100	7.5	10
10	2	21	1.36	100	6.5	10
11	3	21	1.36	100	6.3	10
12	4	21	1.36	100	6.1	10
13	5	21	1.36	100	6.1	10
14	6	21	1.36	100	6.1	10
15	3	21	1.2	100	5.7	10
16	3	21	1.4	100	6.6	10
17	3	21	1.6	100	7.1	10
18	3	21	1.8	100	7.9	10
19	3	21	2	100	8.4	10

4 RESULTS

4.1 Current-Voltage and Charge-Voltage Measurements

The voltage and current traces are analyzed to gain a qualitative understanding of the plasma formation at the different conditions. Most of the preliminary results underwent such analysis until a reasonable test matrix, as previously discussed, was developed. The main qualitative criteria used for getting an indication of plasma formation are the quantity and magnitude of current spikes. The following plots of the voltage and current traces were simplistically analyzed using this logic: more spikes observed both in quantity and magnitude in the current trace indicate more plasma generation.

The energy and electrical power were calculated based upon the QV measurements. Figure 4.1 is an example of a plot of the voltage at the capacitor, V_c, versus the voltage at the exposed electrode, V_t. The area inside of the enclosed region equals the energy [8]. This was calculated by performing a line integral around the region. The power was calculated by multiplying the energy by the frequency of the applied voltage signal.

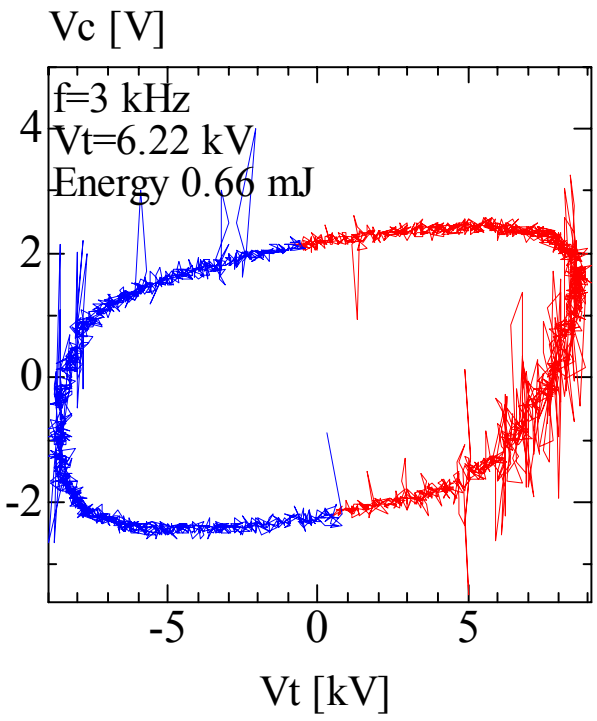

Figure 4.1: Voltage at the Capacitor versus Voltage at the Exposed Electrode

Figures 4.2 and 4.3 depict the effect created by a change in the frequency of the signal. The dielectric strength is 10 kV, and the ballast resistance is set to 100 kOhm. The voltage at the function generator is set to 1.36 V_{RMS}, which corresponds to a voltage applied to the exposed electrode of about 6.4 kV_{RMS} for the frequency at 2 kHz and about 5.8 kV_{RMS} for the frequency at 5 kHz. A comparison of the two plots indicates that as the frequency increased, the quantity of current spikes increased significantly while the magnitude of spikes only slightly increased. The energy generally decreased as the frequency increased, as shown in Figure 4.4. However, the electrical power increased virtually linearly with the frequency (Figure 4.5) which agrees with the qualitative results.

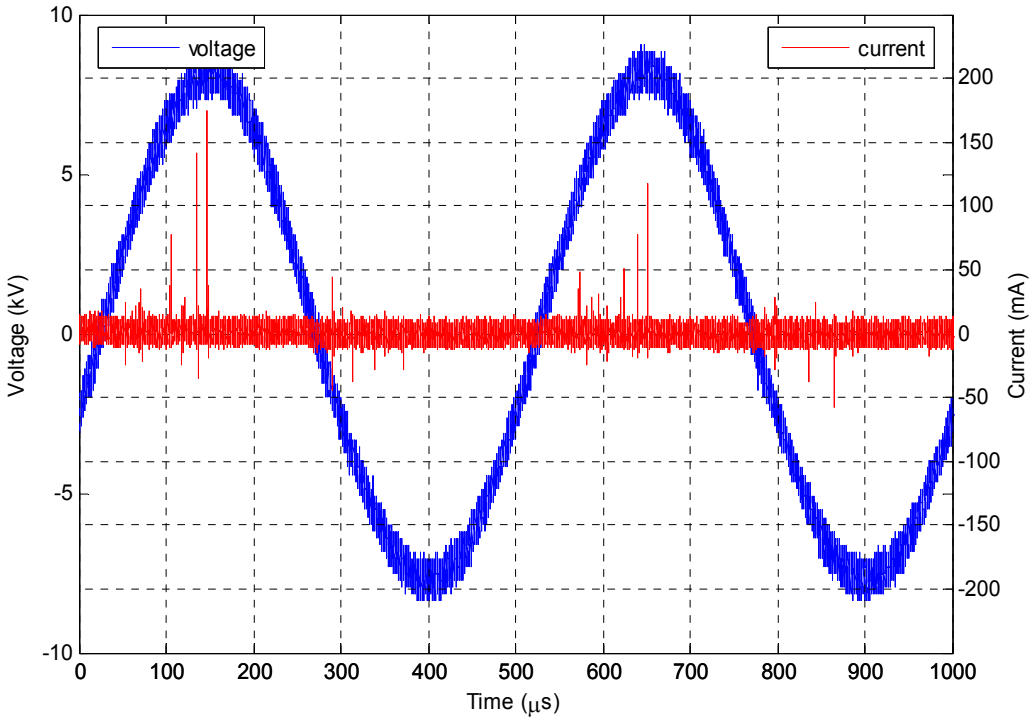

Figure 4.2: Voltage and Current Trace with Frequency of Signal Set to 2 kHz

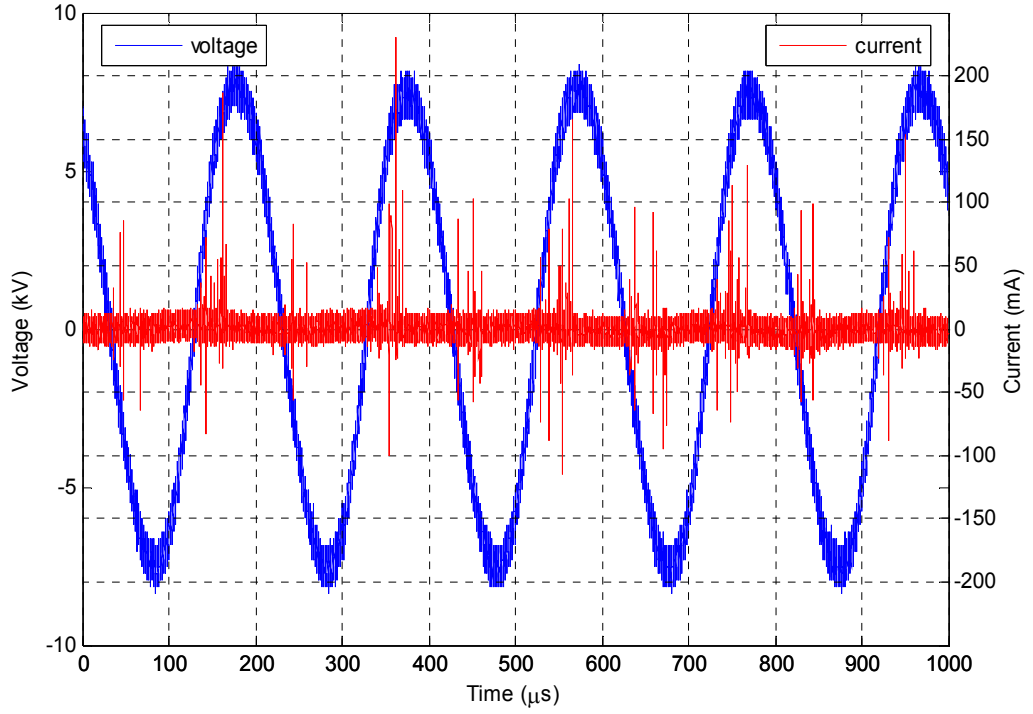

Figure 4.3: Voltage and Current Trace with Frequency of Signal Set to 5 kHz

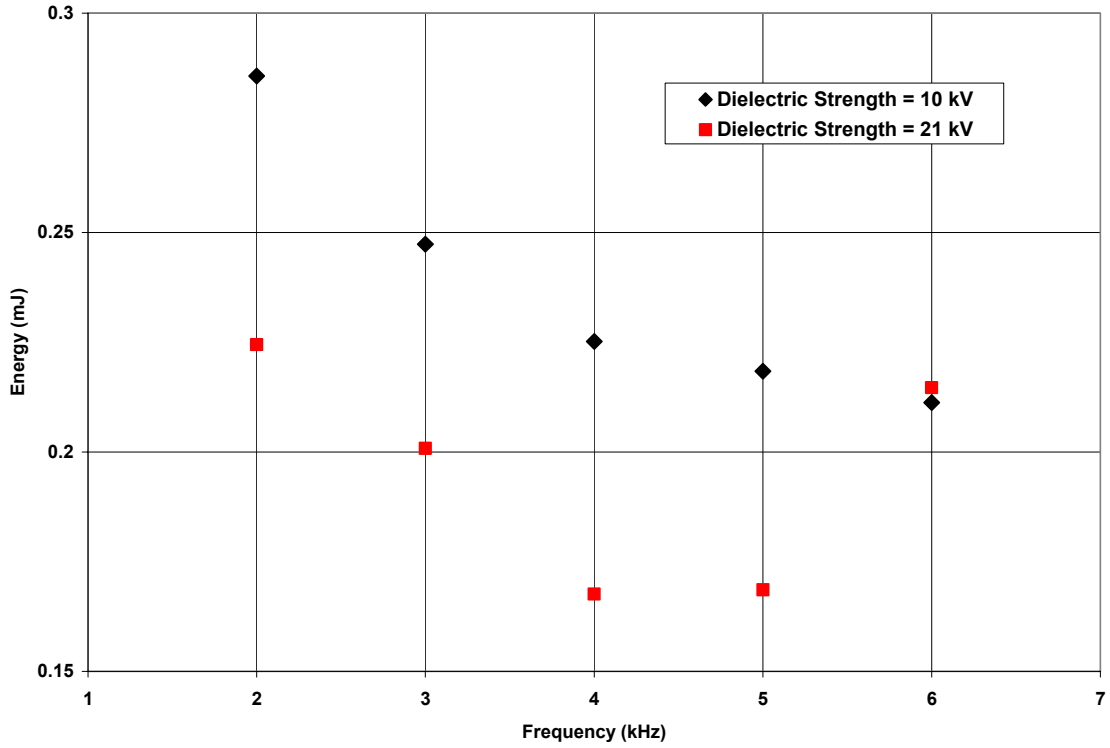

Figure 4.4: Energy Corresponding to Varied Frequency

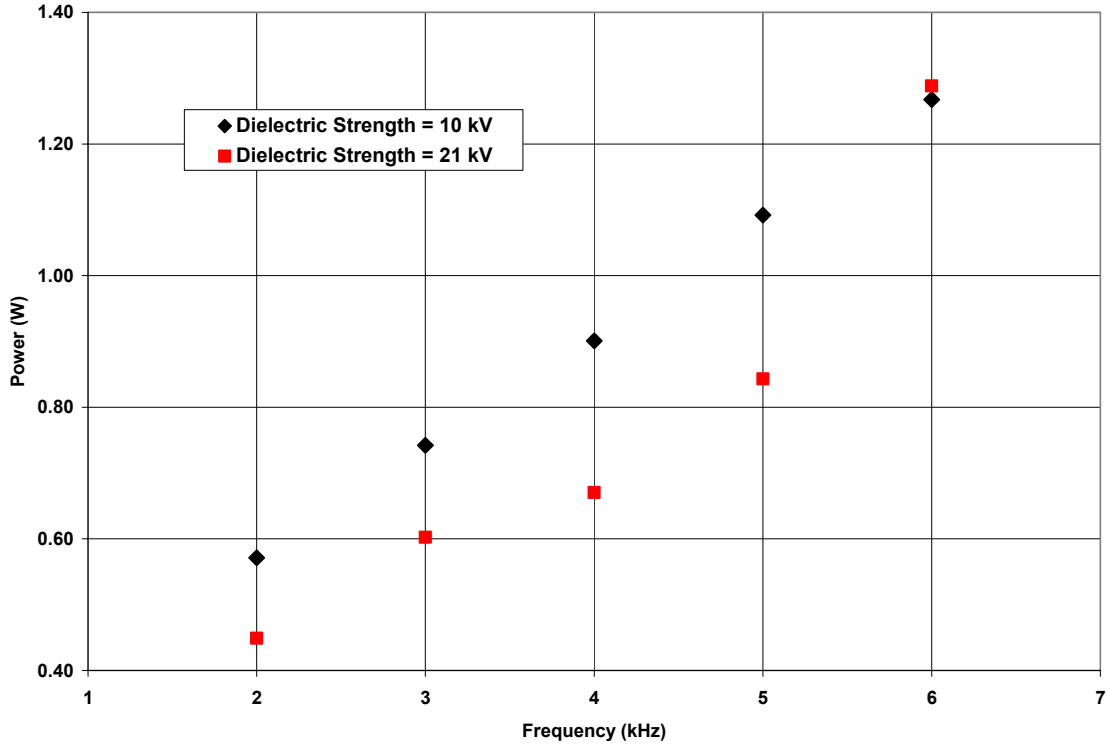

Figure 4.5: Electrical Power Corresponding to Varied Frequency

Figures 4.6 and 4.7 depict the effect of a change in the voltage of the signal. In this case, the dielectric strength is 10 kV, the ballast resistance is 100 kOhm, and the frequency is 3 kHz. Figure 4.6 shows the voltage and current traces when the voltage at the function generator is 1.15 V_{RMS}, which corresponds to a voltage applied to the exposed electrode at about 5.2 kV_{RMS}. Figure 4.7 shows the traces when the voltage at the function generator is set to 1.60 V_{RMS}, which corresponds to a voltage applied to the exposed electrode of about 6.9 kV_{RMS}. The two plots show that as the voltage increases, the quantity and magnitude of the current spikes increases. This indicates more plasma formation.

The electrical energy and power as a function of the applied voltage are shown in Figure 4.8 and Figure 4.9, respectively. Dependence of energy on root-mean-squared voltage applied to the exposed electrode is cubic, which agrees with the results obtained by Pons et al [8].

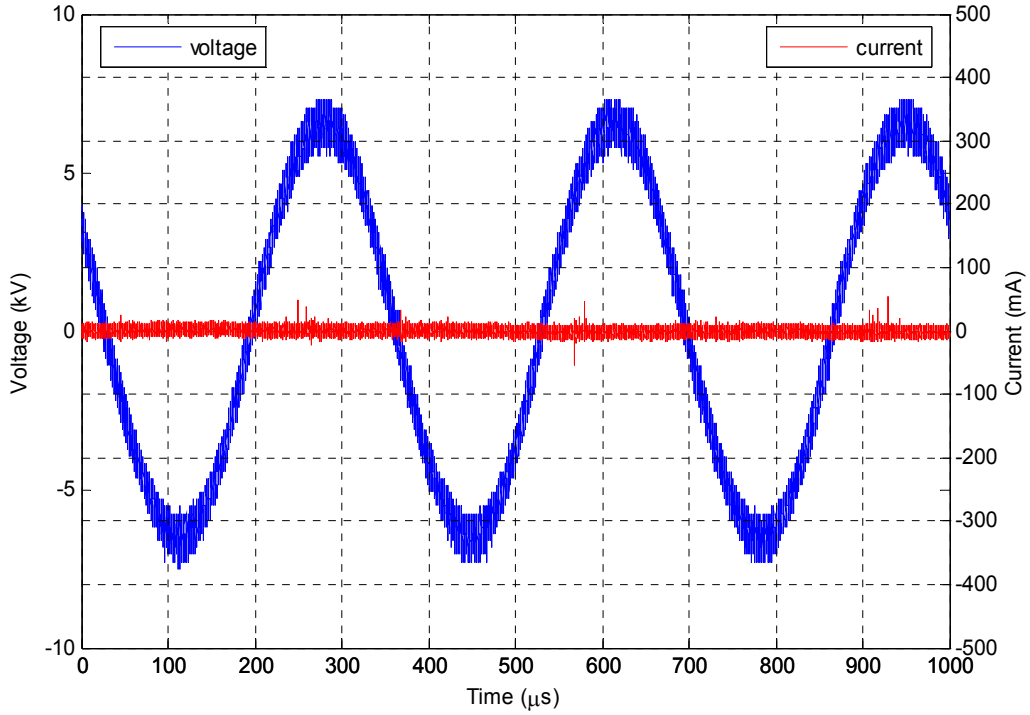

Figure 4.6: Voltage and Current Trace with Voltage at Exposed Electrode at 5.2 kV_{RMS}

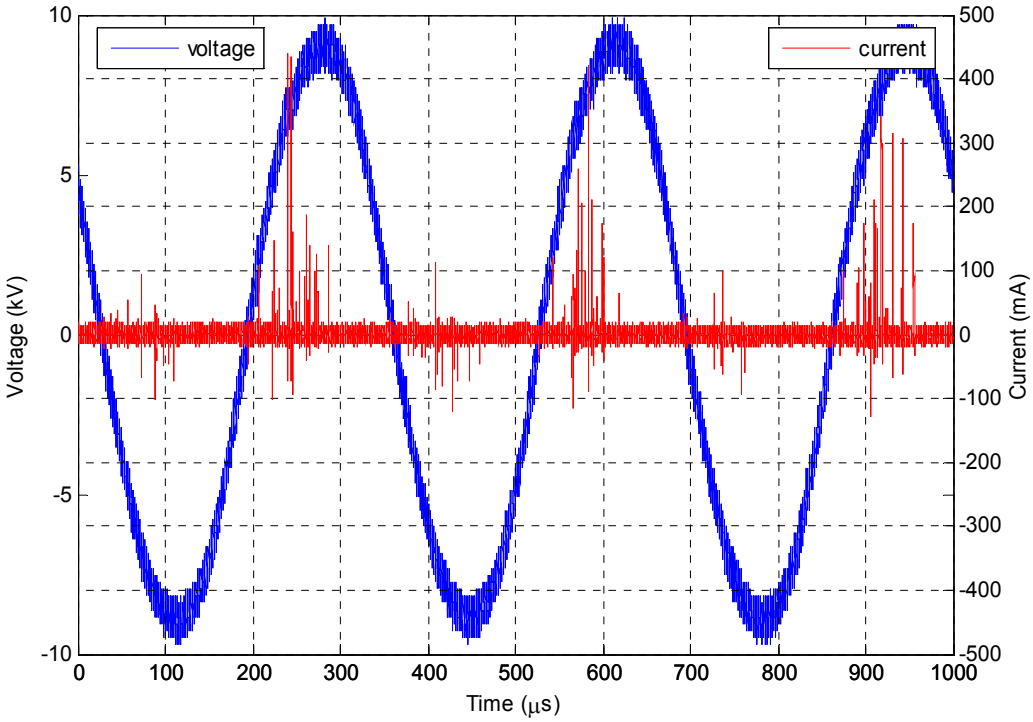

Figure 4.7: Voltage and Current Trace with Voltage at Exposed Electrode at 6.9 kV_{RMS}

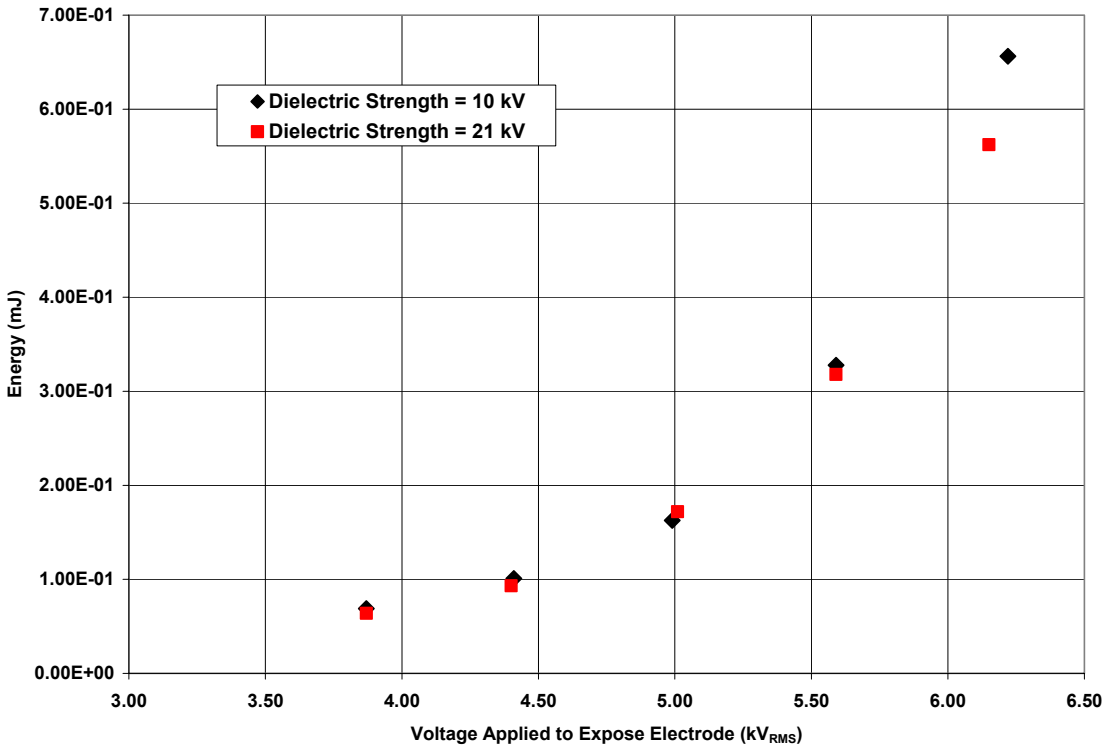

Figure 4.8: Energy Corresponding to Varied V_{RMS} at Exposed Electrode

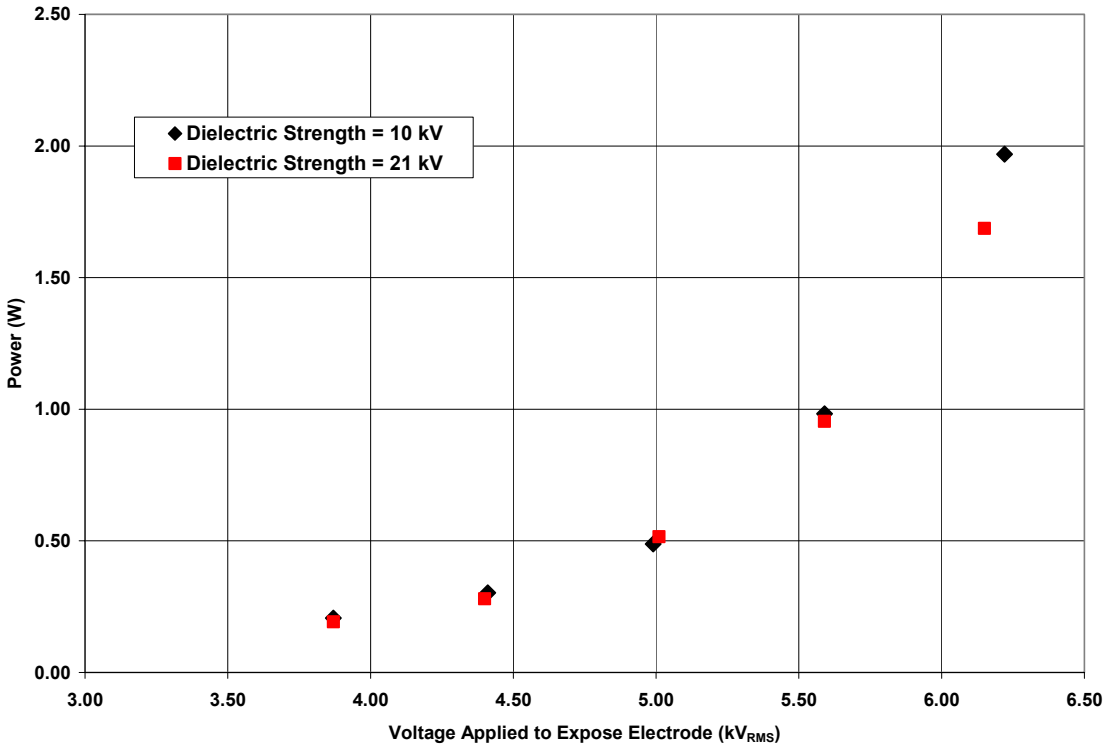

Figure 4.9: Electrical Power Corresponding to Varied V_{RMS} at Exposed Electrode

Figures 4.10 and 4.11 illustrate the effect of a change in the dielectric strength. The ballast resistance is 100 kOhm, and the frequency is 3 kHz. In Figure 4.10, the dielectric strength is 10 kV, and the voltage at the function generator is 1.36 V_{RMS}, which corresponds to a voltage applied to the exposed electrode of about 6.1 kV_{RMS}. In Figure 4.11, the dielectric strength is 21 kV, and the voltage at the function generator is set to 1.36 V_{RMS}, which corresponds to a voltage applied to the exposed electrode of about 5.9 kV_{RMS}. No noticeable change occurred between the two dielectrics used in regard to the quantity and magnitude of the current spikes. This agrees with the small differences seen in electrical power depicted previously in Figure 4.9. However, one point of interest is that the thicker, stronger dielectric of 21 kV is not as susceptible to arcing as the 10 kV dielectric.

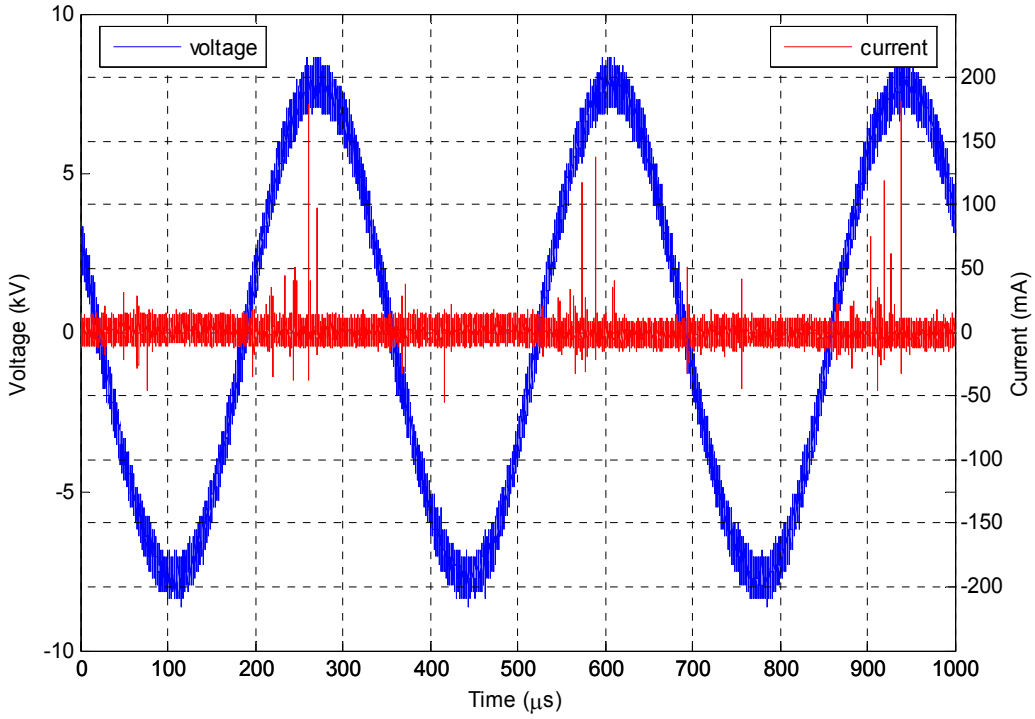

Figure 4.10: Voltage and Current Trace with Dielectric Strength of 10 kV

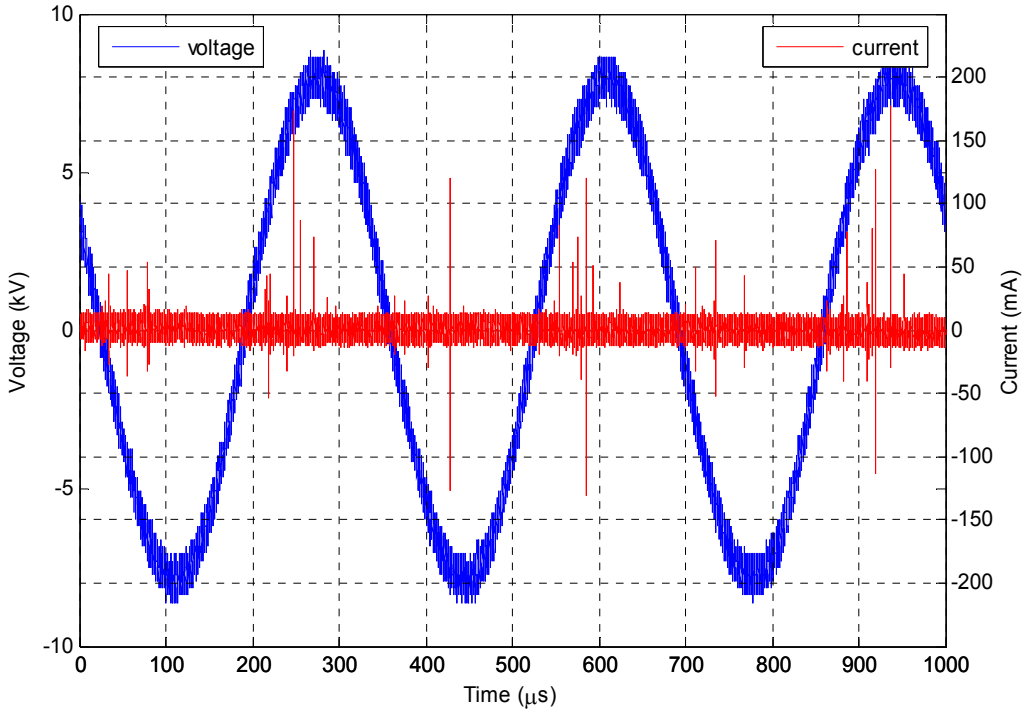

Figure 4.11: Voltage and Current Trace with Dielectric Strength of 21 kV

Figures 4.12 and 4.13 show how a change in the ballast resistance effects plasma formation. The frequency is 3 kHz, and the dielectric with strength of 21 kV is used. Figure 4.12 shows the current and voltage traces with a ballast of 100 kOhm. The function generator is 1.36 V_{RMS}, which corresponds to a voltage applied to the exposed electrode of about 5.9 kV_{RMS}. Figure 4.13 depicts the current and voltage traces with a ballast of about 600 kOhm. The function generator is set to 1.36 V_{RMS}, which corresponds to a voltage applied to the exposed electrode of about 5.0 kV_{RMS}. Figure 4.14 shows that the energy decreased as the ballast increased. The three plots indicate that plasma formation is greater at lower ballast resistance since higher ballast decreases the voltage applied to the exposed electrode. Therefore, an interesting future testing would be to maintain a constant voltage at the exposed electrode while recording the effect of varying the ballast resistance.

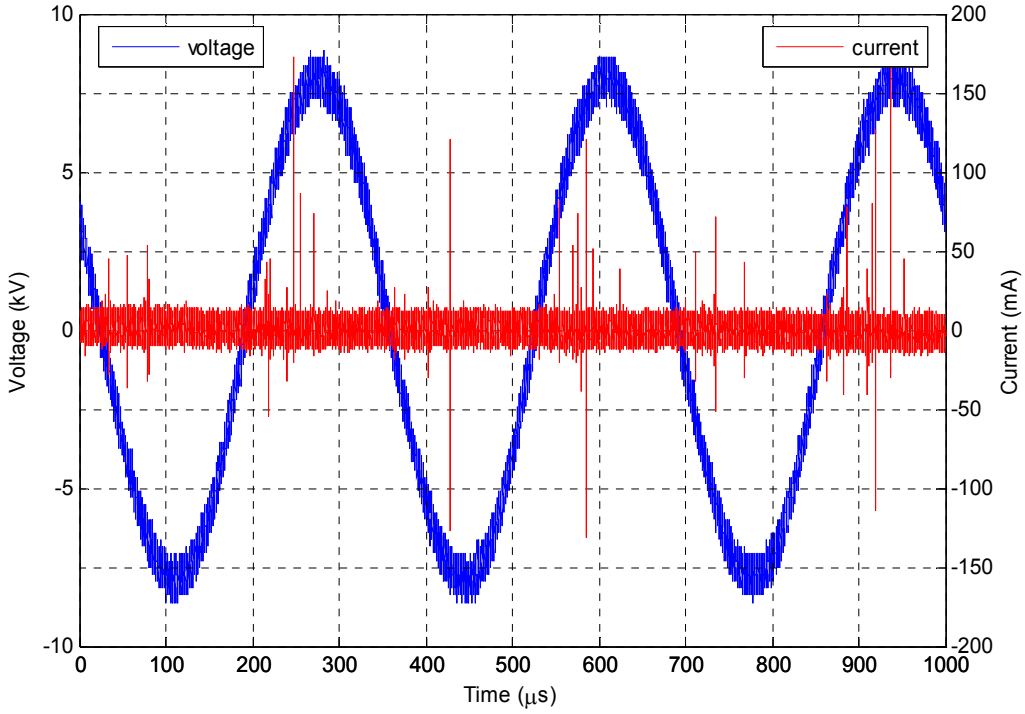

Figure 4.12: Voltage and Current Trace with Ballast Resistance Set to 100 kOhm

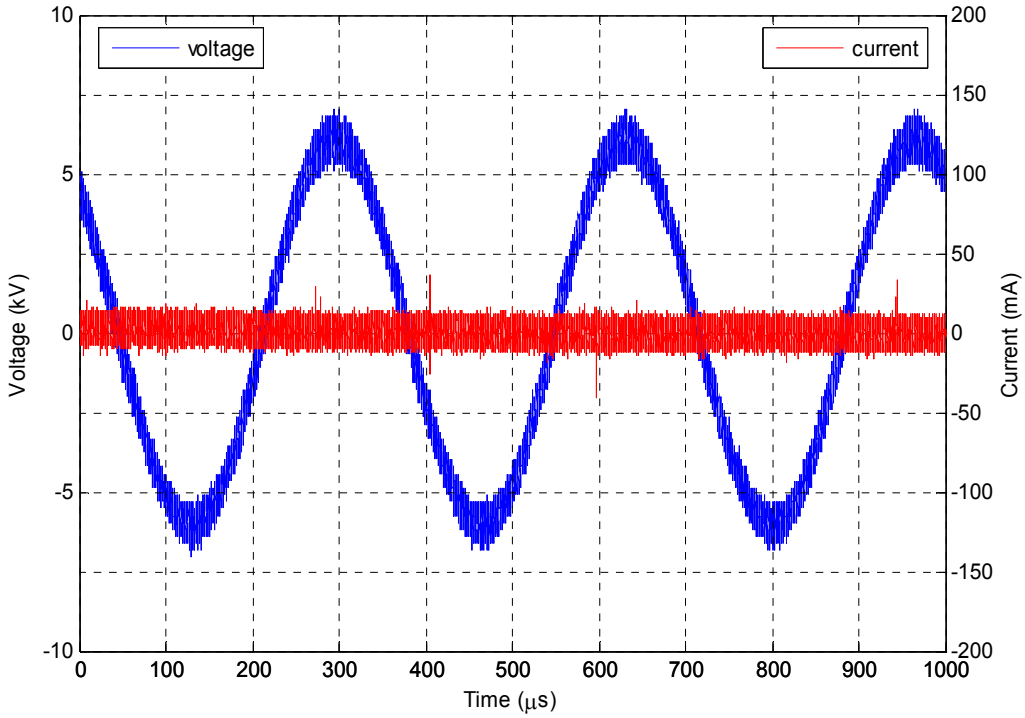

Figure 4.13: Voltage and Current Trace with Ballast Resistance Set to 600 kOhm

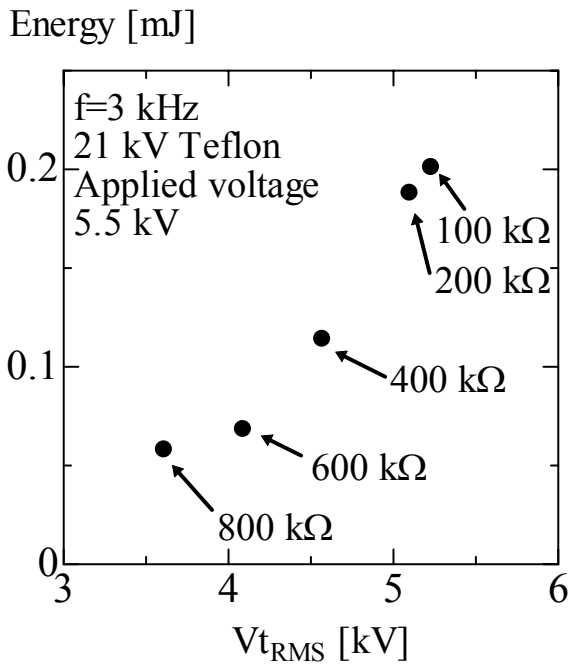

Figure 4.14: Energy Corresponding to Varied Ballast Resistance

4.2 Particle Image Velocimetry

The trends deduced from the PIV measurements agree with those which were displayed in the IV and QV measurements. The general relationships are the following: an increase in frequency, with constant applied voltage, results in an increase in induced velocity. Similarly, an increase in applied voltage, with constant frequency, yields an increase in induced velocity.

Figures 4.15-4.17 depict the relationship between the total induced velocity and varying the frequency. Figures 4.18-4.20 depict the relationship between the streamwise component of the induced velocity and varying the frequency. Figures 4.21-4.23 depict the relationship between the normal component of the induced velocity and varying the frequency.

Figures 4.24-4.26 depict the relationship between the total induced velocity and varying the applied voltage. Figures 4.27-4.29 depict the relationship between the streamwise component of the induced velocity and varying the applied voltage. Figures 4.30-4.32 depict the relationship between the normal component of the induced velocity and varying the applied voltage.

A small schematic of the plasma actuator can be seen at the bottom left of all the following figures in order to show the spatial relation between the induced velocity and the location of the actuator electrodes. The leading edge of the exposed electrode is taken as the reference point for the x-axis and the surface of the test block as the reference point for the y-axis. The color scale corresponds to the total velocity in cm/sec.

For the cases where the frequency is varied, the constant input voltage from the function generator is 1.36 V_{RMS}, which corresponds to applied voltages at the exposed electrode ranging from about 6 to 6.5 kV_{RMS}. Even though the input voltage at the function generator is held constant, there is a slight decrease in the voltage at the exposed electrode as the frequency increases. Namely, a higher applied voltage occurs at a lower frequency. Currently, the reason for this effect is not certain and will be determined with future characterization. For the cases where the applied voltage is varied, the frequency is held constant at 3 kHz.

Three important characteristics seen in the PIV data of the induced flow are (1) the region of maximum total velocity at about 50 mm away from the leading edge of the exposed electrode, (2) the fact that prevailing direction of the induced flow is in the streamwise direction, and (3) the downward suction that occurs at about 8 mm away from the leading edge of the exposed electrode, These three aspects are extremely apparent for

higher frequencies and applied voltages. The 21 kV dielectric is capable of sustaining plasma at a higher applied voltage than the 10 kV dielectric. When about 8 kV_{RMS} was applied to the actuator with the 10 kV dielectric, arcing occurred, burning a hole through the dielectric. The 21 kV dielectric actuator has the capability to withstand higher applied voltages and thus higher induced velocities.

Comparing the maximum total velocity to the maximum streamwise component of velocity, it can be seen that the dominant component of velocity is in the x-direction. Furthermore, the maximum total velocity and maximum streamwise component of velocity occur essentially at the same location. Specifically, these maximum values occur at about 50 to 60 mm away from the leading edge of the exposed electrode and at about 3 to 4 mm above the surface of the actuator. The maximum induced velocity is found to be 145 cm/sec. This occurs with a frequency of 3 kHz, applied voltage of 8.4 kV_{RMS}, and a dielectric with strength of 21 kV (Figure 4.26).

Figures 4.23 and 4.32 show the absolute value of the maximum normal component of velocity. In reality this value is negative, which indicates a downward direction. This depicts the maximum suction that occurs at about 8 mm downstream from the leading edge of the exposed electrode and at about 5 mm above the surface of the actuator.

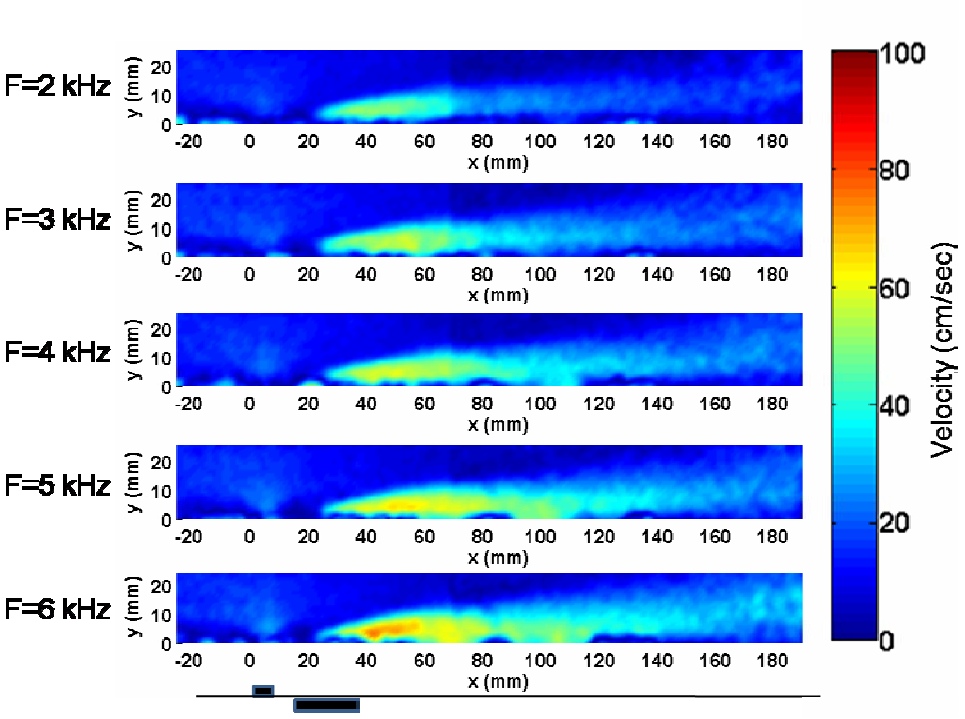

Figure 4.15: Total Induced Velocity with Dielectric Strength of 10 kV and Constant Voltage

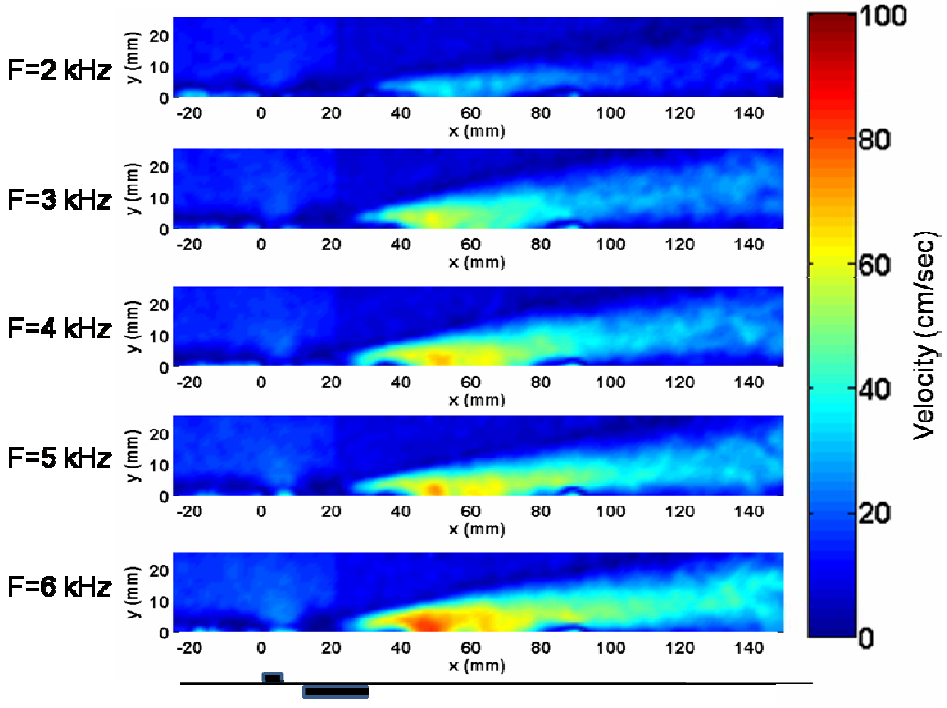

Figure 4.16: Total Induced Velocity with Dielectric Strength of 21 kV and Constant Voltage

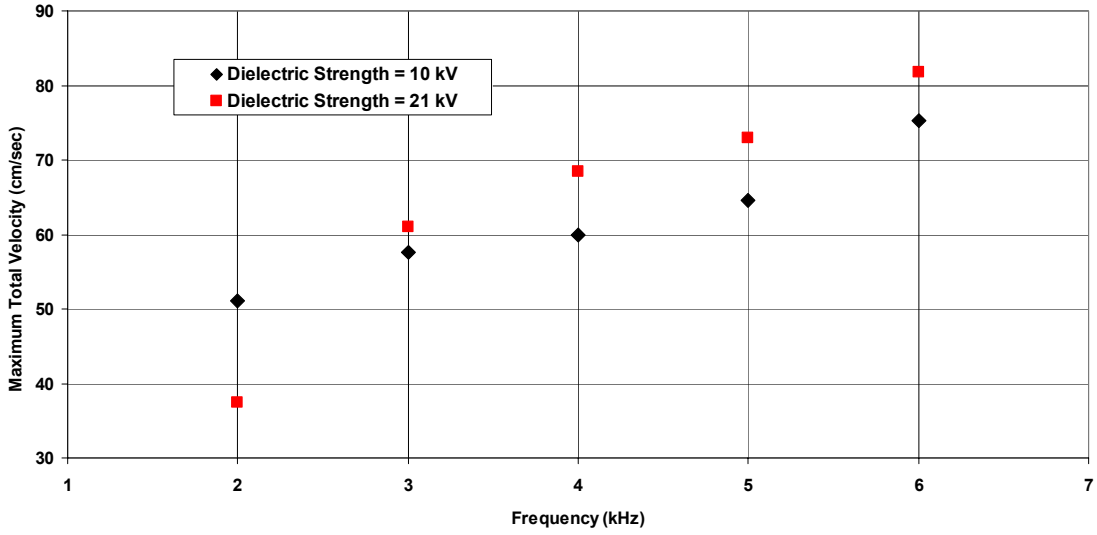

Figure 4.17: Maximum Total Velocity Corresponding to Frequency with Constant Voltage

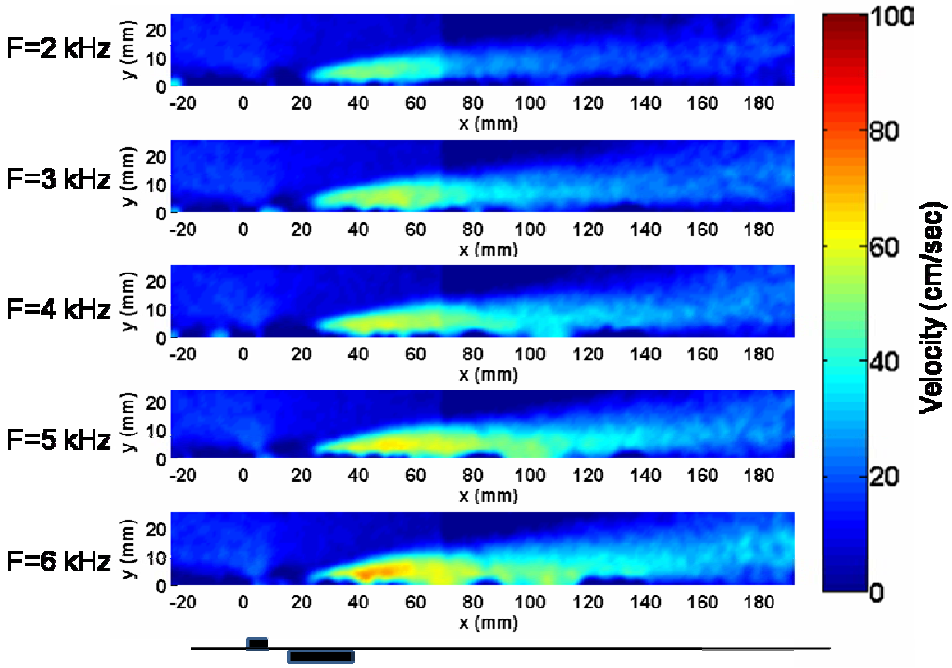

Figure 4.18: Streamwise Velocity U_x with Dielectric Strength of 10 kV and Constant Voltage

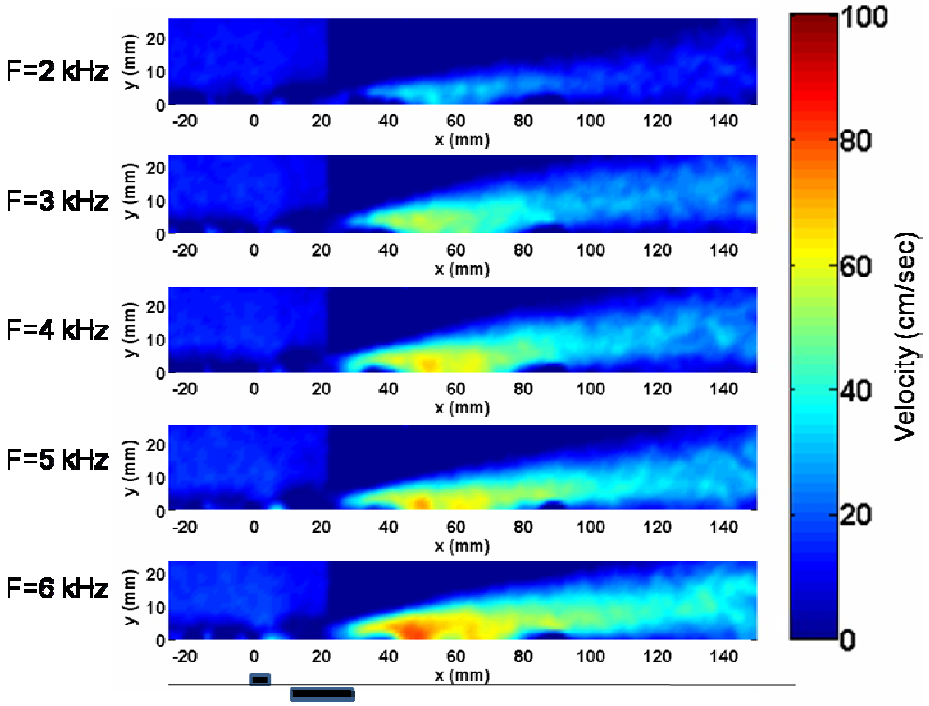

Figure 4.19: Streamwise Velocity U_x with Dielectric Strength of 21 kV and Constant Voltage

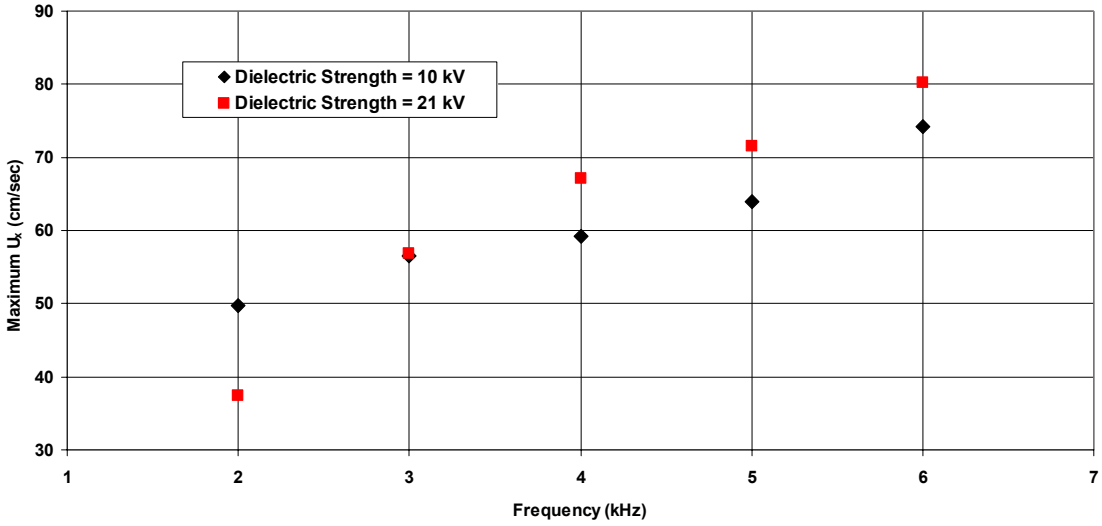

Figure 4.20: Maximum Streamwise Velocity U_x Corresponding to Frequency with Constant Voltage

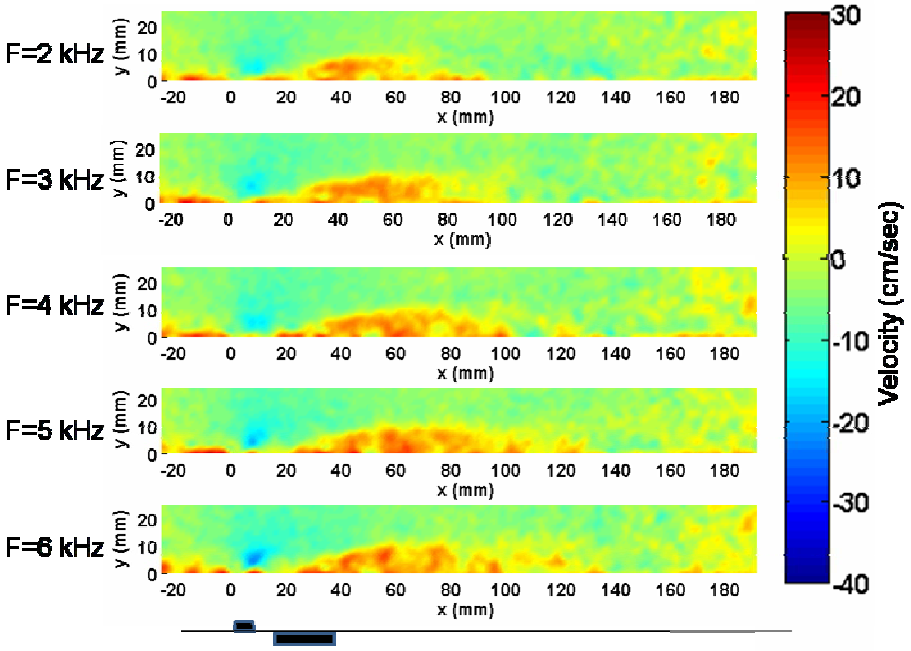

Figure 4.21: Normal Velocity V_y with Dielectric Strength of 10 kV and Constant Voltage

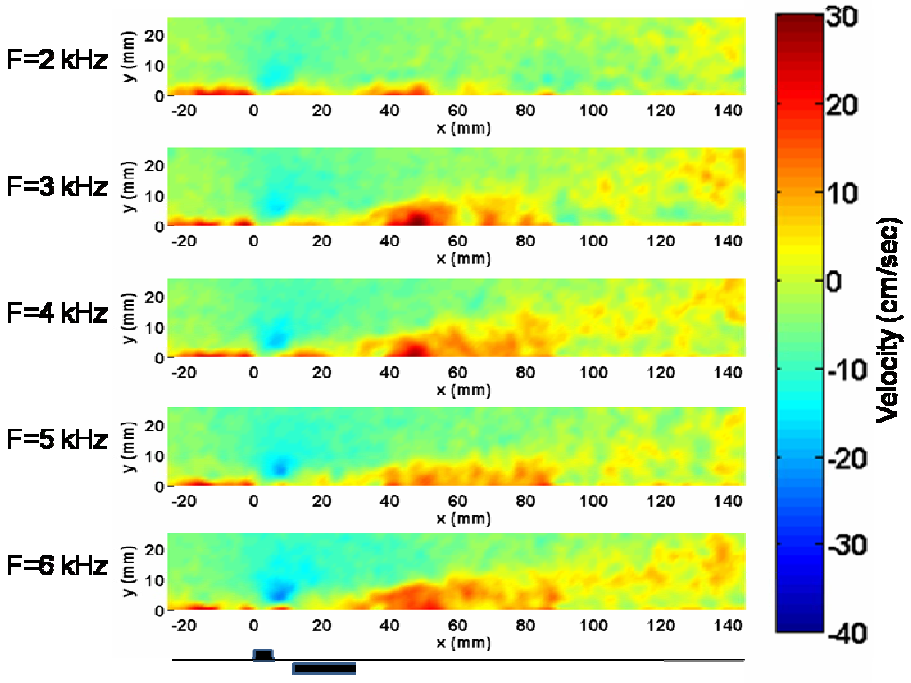

Figure 4.22: Normal Velocity V_y with Dielectric Strength of 21 kV and Constant Voltage

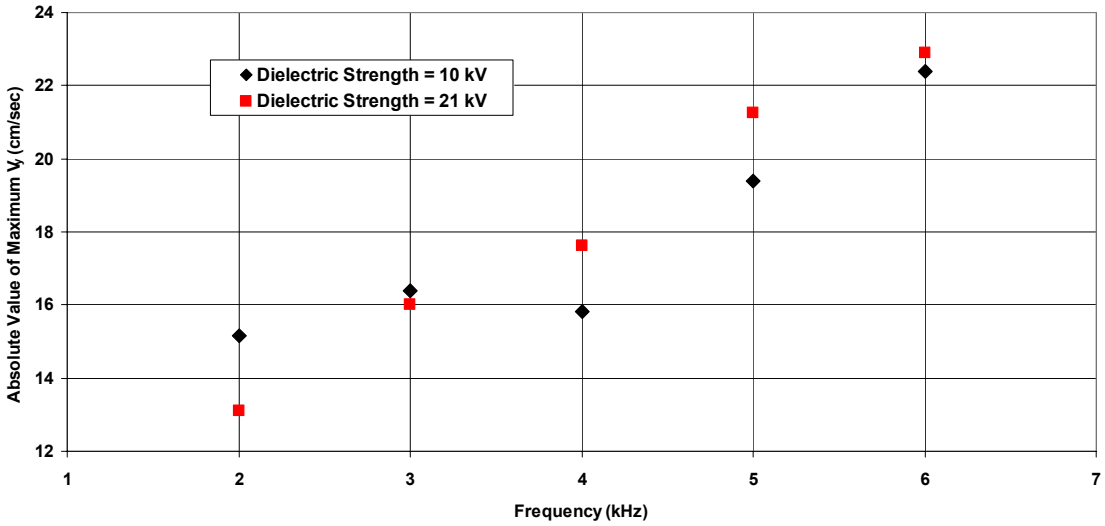

Figure 4.23: Maximum Normal Velocity V_y Corresponding to Frequency with Constant Voltage

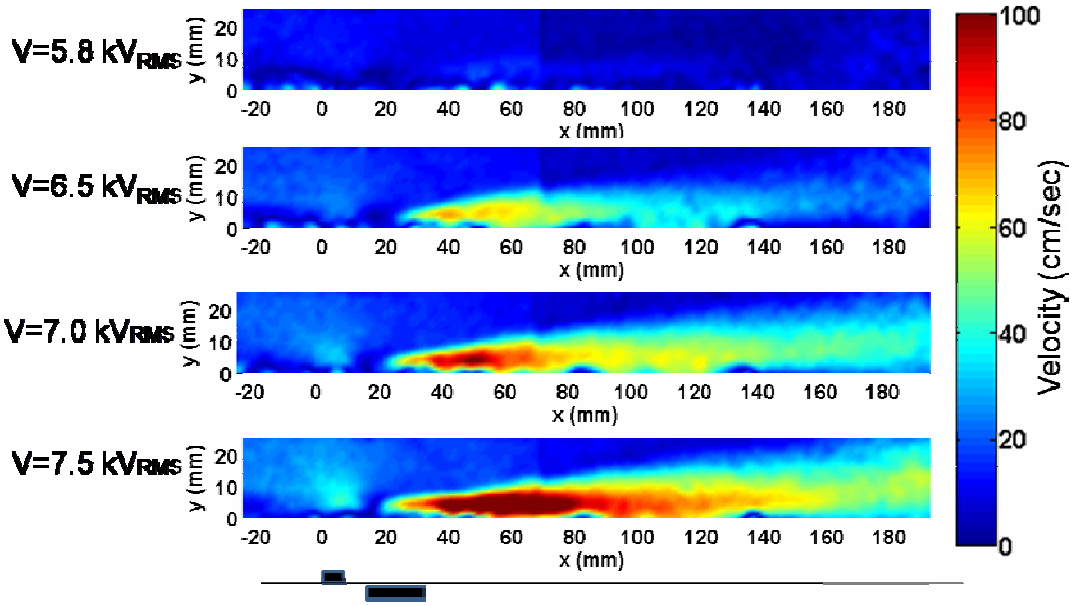

Figure 4.24: Total Induced Velocity with Dielectric Strength of 10 kV and Constant Frequency

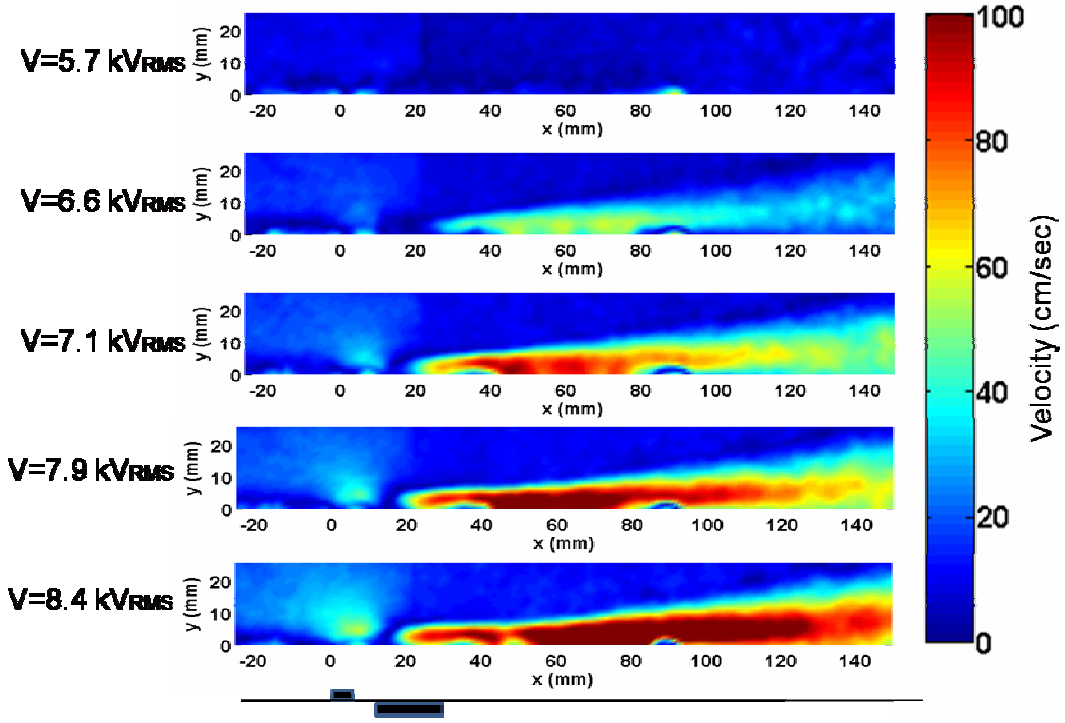

Figure 4.25: Total Induced Velocity with Dielectric Strength of 21 kV and Constant Frequency

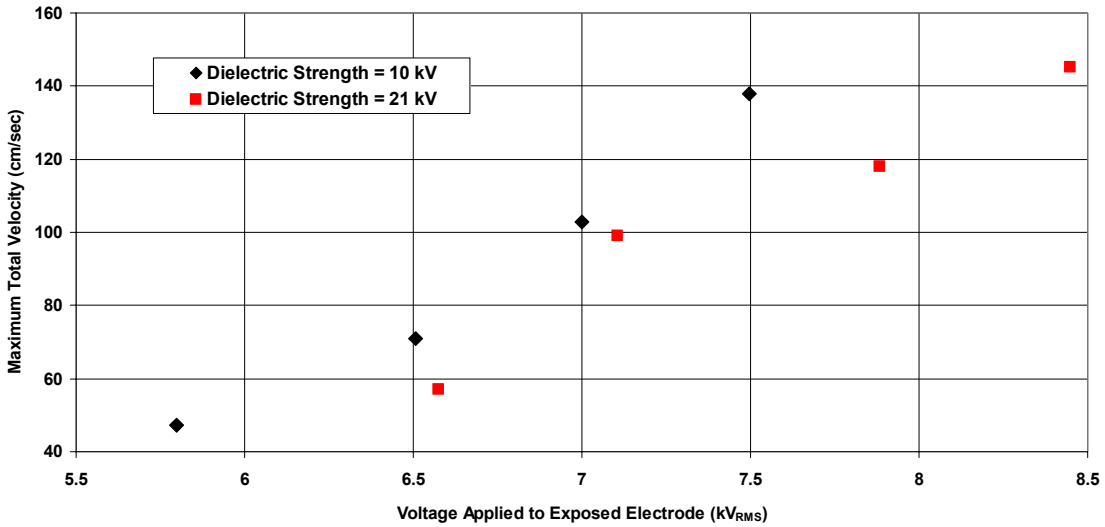

Figure 4.26: Maximum Total Velocity Corresponding to Applied Voltage with Constant Frequency

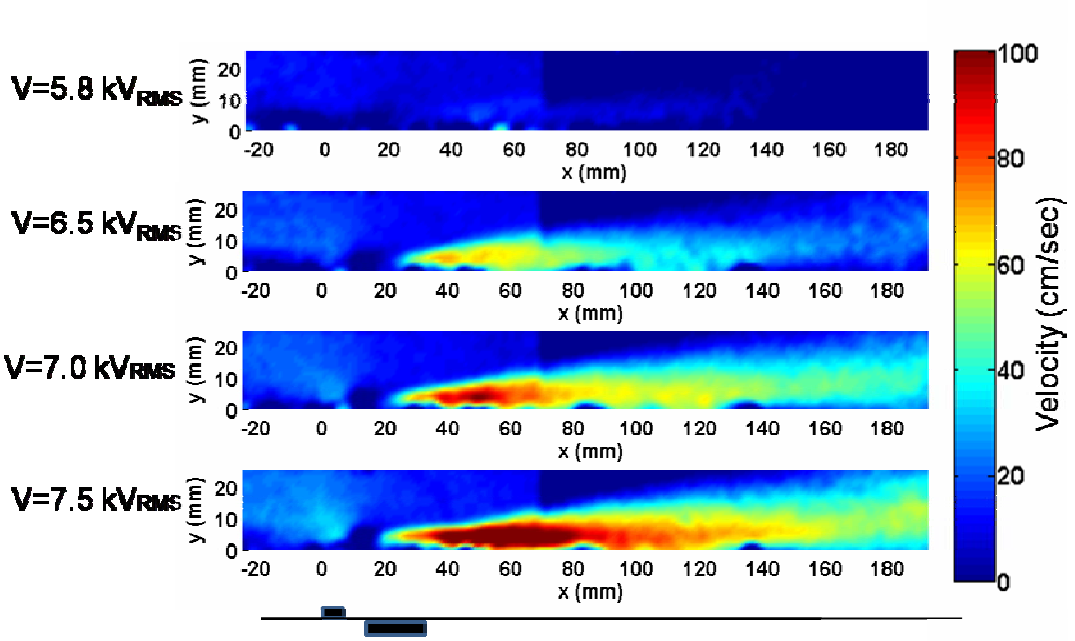

Figure 4.27: Streamwise Velocity U_x with Dielectric Strength of 10 kV and Constant Frequency

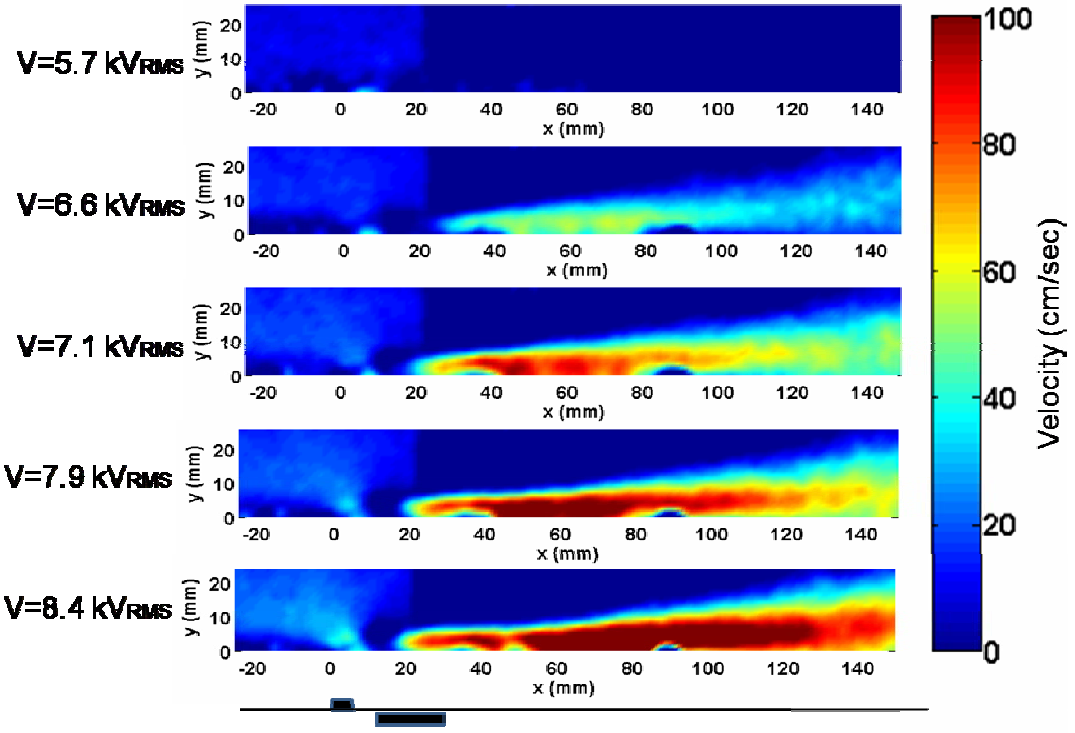

Figure 4.28: Streamwise Velocity U_x with Dielectric Strength of 21 kV and Constant Frequency

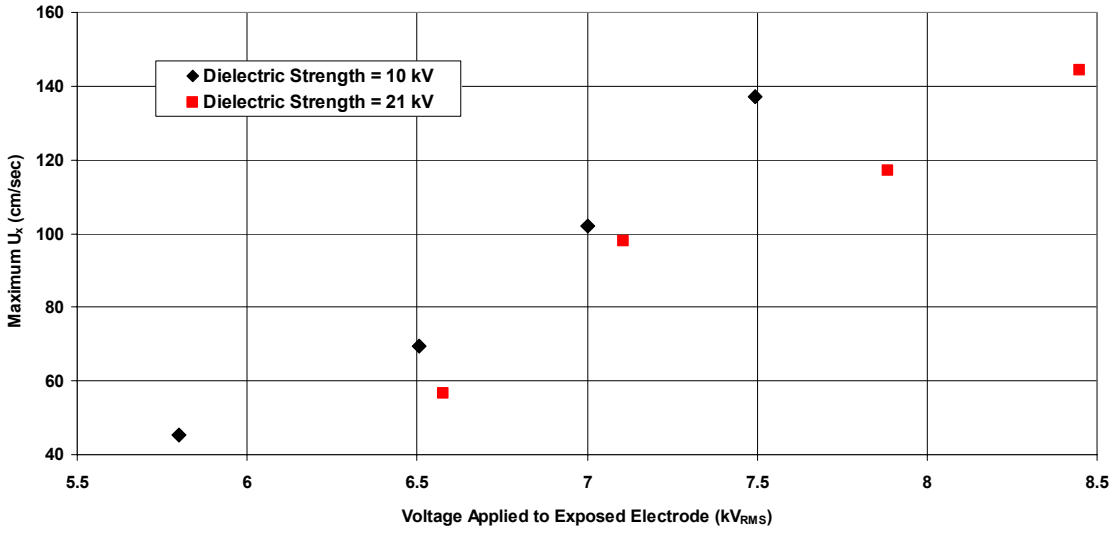

Figure 4.29: Maximum Streamwise Velocity, U_x, Corresponding to Applied Voltage with Constant Frequency

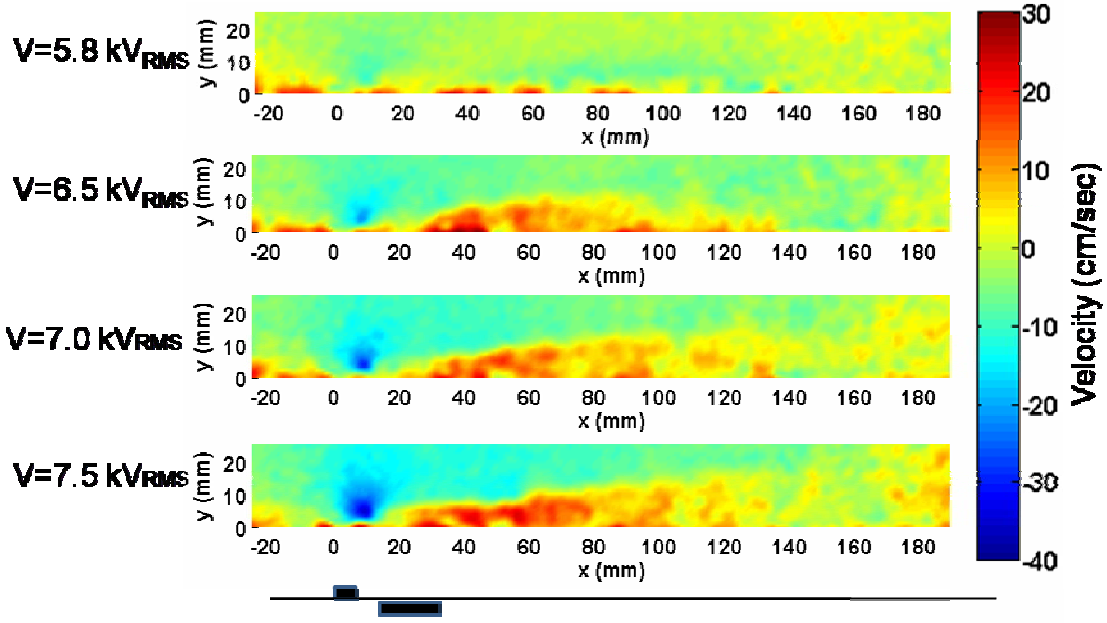

Figure 4.30: Normal Velocity V_y with Dielectric Strength of 10 kV and Constant Frequency

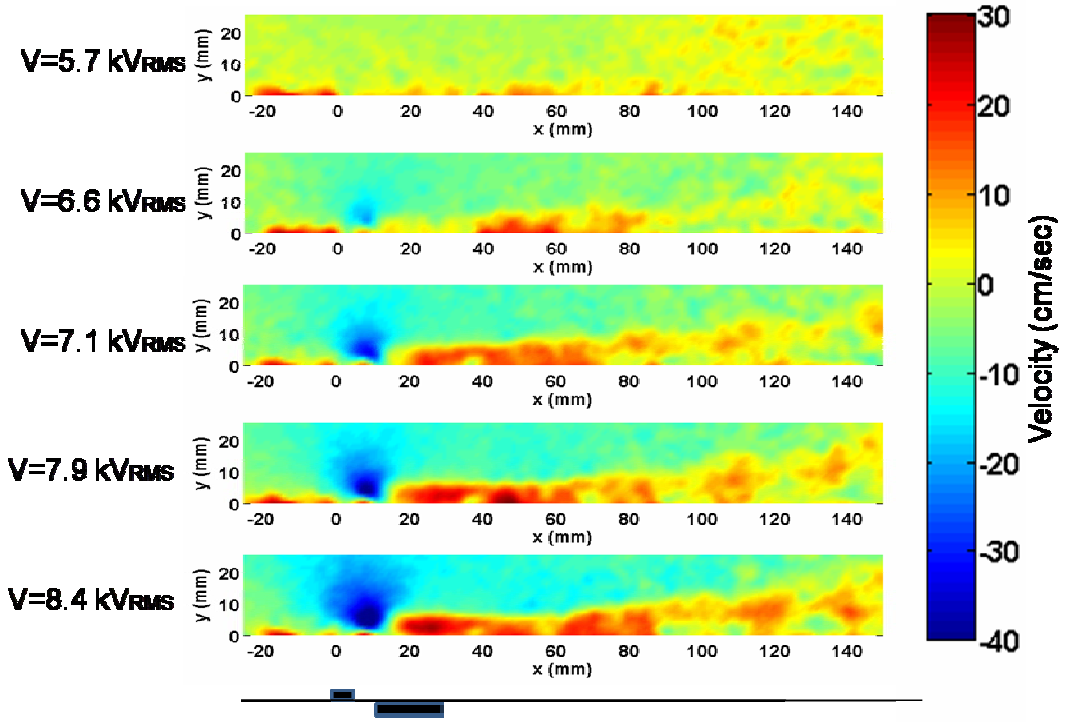

Figure 4.31: Normal Velocity V_y with Dielectric Strength of 21 kV and Constant Frequency

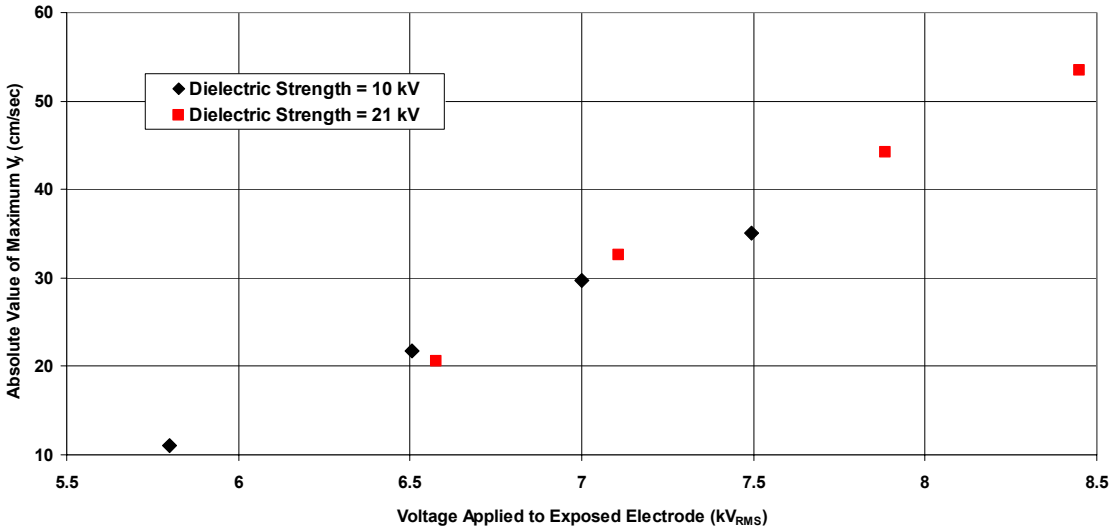

Figure 4.32: Maximum Normal Velocity, V_y, Corresponding to Applied Voltage with Constant Frequency

5 CONCLUSION AND FUTURE WORK

A design for DBD plasma actuators was developed and characterized using recommendation from existing literature. Several parameters that affect the actuators flow inducing features were analyzed to attain a better understanding of the setup that will be applied to a high-lift airfoil. These parameters included the frequency and voltage of the signal, the dielectric strength, and the ballast resistance.

The analysis performed on the actuators included a qualitative examination of the IV measurements, calculations of the electrical energy and power from the QV measurements, and a determination of the magnitude and location of the maximum velocity and its components from the PIV measurements. The general trend shows that stronger plasma formation and a higher induced velocity occur at the higher frequencies, higher applied voltages, stronger dielectrics, and lower ballast resistances.

When considering the current traces of IV measurements, this trend was deduced based upon the microdischarges indicated by current spikes, which are indicative of plasma formation. The calculations from the QV measurements showed that the energy and electrical power increased with an increase in the voltage and frequency, stayed relatively the same with the different dielectric strengths, and decreased with an increase in ballast.

These basic trends agree with existing literature. Additionally, two general characteristics of the actuator that are consistent with literature are that the direction of induced flow is from exposed electrode to insulated electrode and that the magnitude and location of maximum induced velocity are relatively the same. One particular point that is inconsistent is that the magnitude of current spikes, as seen in the IV measurements,

are one order of magnitude greater than that which is seen in the literature. This is most likely due to the ballast resistance not being high enough.

The PIV results showed that higher induced velocities were achieved with higher frequency and voltage. The 10 kV dielectric was more susceptible to arcing than the 21 kV dielectric. The magnitude and location of the maximum total velocity and streamwise component of velocity were virtually the same. This shows that the flow inducing effects occur in the correct direction, namely, in the direction of external flow. This fact renders the plasma actuator as suitable for introducing momentum into the boundary layer of flow passing over an airfoil for the purpose of delaying separation. However, the effectiveness of this application requires much more research.

Future studies should consist of better characterizing the DBD plasma actuators. The PIV measurements and electrical properties need be tested simultaneously and both types of measurements need to be performed to ensure repeatability. Furthermore, experiments at higher applied voltages and a large frequency range should be tested to quantify trends. Due to the discrepancy between the magnitude of the current spikes in comparison to current literature, the effect of the ballast needs to be investigated. Different dielectric materials and their effect on the induced flow should be tested as well. Other interesting experiments should include different input waveforms and testing multiple actuators in series in hopes of attaining an additive effect of the induced flow. The study of these parameters should provide a better actuator design, which can subsequently be applied to a high-lift airfoil for flow separation control studies.

REFERENCES

1. Corke, T. and Post, M., Overview of Plasma Flow Control: Concepts, Optimization, and Applications. AIAA Paper 2005-0563.
2. Forte, M., Jolibois, J., Moreau, E., and Touchard, G., Optimization of Dielectric Barrier Discharge Actuator by Stationary and Non-Stationary Measurements of the Induced Flow Velocity – Application to Airflow Control. AIAA Paper 2006-2863.
3. Santhanakrishnan, A., Jacob, J., Suzen, Y., Flow Control Using Plasma Actuators and Linear/Annular Plasma Syntheic Jet Actuators. AIAA Paper 2006-3033.
4. Font, G., Plasma Actuators: A Particle Perspective. Workshop on Plasma Actuators, US Air Force Academy. Nov 8-9th, 2006.
5. Enloe, C., McLaughlin, T., VanDyken, R., Kachner, K., Jumper, E., Corke, T., Mechanisms and Responses of a Single Dielectric Barrier Plasma Actuator: Plasma Morphology. AIAA Journal, Vol. 42, No. 3, March 2004.
6. Enloe, C., McLaughlin, T., Font, G., Baughn, J., Parameterization of Temporal Structure in the Single-Dielectric-Barrier Aerodynamic Plasma Actuator. AIAA Journal, Vol. 44, No. 6, June 2006.
7. Little, J., An Experimental Investigation of Subsonic Cavity Flows without and with Forcing. A Thesis Presented in Partial Fulfillment of the Requirements for the Degree Master of Science in the Graduate School of The Ohio State University. 2005.
8. Pons, J., Moreau, E., and Touchard, G., Asymmetric surface dielectric barrier discharge in air at atmospheric pressure: electrical properties and induced airflow characteristics, J. Phys. D: Applied Physics, 38, pp. 3635-3642, 2005.